Author Manuscript

Author Manuscript

Author Manuscript

Author Manuscript

HHS Public Access

Author manuscript

Cell Rep. Author manuscript; available in PMC 2019 November 25.

Published in final edited form as:

Cell Rep. 2018 November 20; 25(8): 2177–2191.e7. doi:10.1016/j.celrep.2018.10.082.

Plasminogen activator inhibitor-1 promotes the recruitment and polarization of macrophages in cancer

Marta Helena Kubala[1,2], **Vasu Punj**[4], **Veronica Rae Placencio-Hickok**[1,2], **Hua Fang**[1,2], **G. Esteban Fernandez**[2], **Richard Sposto**[1,2,5], **Yves Albert DeClerck**[1,2,3]

[1]Division of Hematology, Oncology and Blood and Bone Marrow Transplantation, Department of Pediatrics, University of Southern California, Los Angeles, CA, 90033, USA;

[2]The Saban Research Institute of Children's Hospital, Los Angeles, CA, 90027, USA;

[3]Department of Biochemistry and Molecular Medicine, University of Southern California, Los Angeles, CA, 90033, USA;

[4]Division of Hematology, Department of Medicine, University of Southern California, Los Angeles, CA, 90033, USA;

[5]Department of Preventive Medicine, University of Southern California, Los Angeles, CA, 90033, USA.

Summary

Plasminogen activator inhibitor-1 (PAI-1) has a pro-tumorigenic function via its pro-angiogenic and anti-apoptotic activities. Here we demonstrate that PAI-1 promoted the recruitment and M2 polarization of monocytes/macrophages through different structural domains. Its LRP1 interacting domain regulated macrophage migration, while its C-terminal uPA interacting domain promoted M2 macrophage polarization through activation of p38MAPK and NF-κB and induction of an autocrine IL-6/STAT3 activation pathway. We then show in several experiments in mice, that expression of PAI-1 is associated with increased tumorigenicity, increased presence of M2 macrophages, higher levels of IL-6 and increased STAT3 phosphorylation in macrophages. Strong positive correlations between PAI-1, IL-6 and CD163 (M2 marker) expression were also found by meta-analysis of transcriptome data in many human cancers. Altogether, these data provide evidence for a mechanism explaining the paradoxical pro-tumorigenic function of PAI-1 in cancer.

Keywords

Plasminogen activator inhibitor-1 (PAI-1); tumor-associated macrophages; M2 polarization; interleukin 6; STAT3; tumor microenvironment

Address correspondence to: Yves A. DeClerck, declerck@usc.edu.

Author contributions

MHK designed and performed the experiments, analyzed the data, prepared the figures and wrote the manuscript. VP performed the analysis of the TCGA and gene expression array data and generated graphs used in Figure 1 and 3. VRPH contributed to the original concept and initiated experiments described in Figure 1A. HF performed the *in vivo* experiment from which tumor sections were used in Figure 1. RS performed statistical analysis of the *in vivo* and *in vitro* experiments. GEF performed confocal microscopy and analysis of digital images. YAD conceived and overviewed the project, obtained funding, designed the experiments, analyzed the data and wrote the manuscript. All authors report no conflicts of interest.

Author Manuscript Author Manuscript Author Manuscript Author Manuscript

Introduction

Plasminogen activator inhibitor-1 (PAI-1; aka SERPIN E1) is overexpressed in a variety of tumors, and is a strong predictor of poor clinical outcome and poor response to therapy (Duffy et al., 2016; Mengele et al., 2010). Such function has been linked to its pro-angiogenic and anti-apoptotic activities. The pro-angiogenic activity of PAI-1 stems from its protease-inhibiting (Bajou et al., 2001) and vitronectin-binding properties. PAI-1 protects endothelial cells (EC) from plasmin-mediated Fas-ligand (Fas-L) cleavage and Fas-L-dependent extrinsic apoptosis (Bajou et al., 2008), and through its vitronectin-binding domain, promotes the detachment of EC from vitronectin and their migration toward fibronectin-rich tissues (Isogai et al., 2001). PAI-1 also has an anti-apoptotic activity against tumor cells and protects them from drug-induced apoptosis (Fang et al., 2012).

The pleiotropic functions of PAI-1 stem from its ability to interact with a number of proteins including urokinase-type plasminogen activator (uPA), the low-density lipoprotein receptor-related protein 1 (LRP1), and vitronectin. PAI-1 inhibits uPA through binding of the reactive center loop to uPA active site and formation of a stable complex (Huntington et al., 2000). This interaction involves two residues in the C-terminal domain of PAI-1: T333 and A335 (Lawrence et al., 2000). uPA receptor (uPAR)-bound PAI-1 interacts with LRP1 via basic residues located in helices D and E, which leads to internalization of the entire complex (Czekay et al., 2011). Free PAI-1 also binds to LRP1 through its N-terminal domain, in which residues R76 and I91 play a necessary role (Stefansson et al., 1998). Binding of the N-terminal domain of PAI-1 to vitronectin interferes with integrin-mediated cell adhesion (Seiffert et al., 1994).

Increasing evidence points towards a contributory function of PAI-1 in inflammation. PAI-1 promotes inflammation induced by cigarette smoke extracts in alveolar epithelial cells (Xu et al., 2009) and stimulates the recruitment of interstitial myofibroblasts and macrophages post kidney injury in mice (Oda et al., 2001). These observations raise the possibility that the contribution of PAI-1 to inflammation could play a role in its pro-tumorigenic function, a question not previously explored.

Tumor-associated macrophages (TAM) play a central role in inflammation in cancer. They have a spectrum of polarization types, ranging from M1-classically activated anti-tumorigenic macrophages expressing high levels of IL-1, IL-12, and inducible nitrous oxide synthase (iNOS) to M2-alternatively activated macrophages that have immunosuppressive and pro-tumorigenic functions having high levels of expression of IL-10, Arginase, CD163, and CD206 (Murray et al., 2014). Here, we have investigated whether PAI-1 could affect macrophage migration and polarization as part of its pro-tumorigenic activity within the tumor microenvironment (TME).

Results

Decreased presence of TAM in xenotransplanted tumors in the absence of PAI-1

We previously reported that PAI-$1^{-/-}$ mice (defined as host [H] -) engrafted with HT-1080 human fibrosarcoma or A549 human lung cancer cells in which PAI-1 expression was

Author Manuscript Author Manuscript Author Manuscript Author Manuscript

knocked down (defined as tumor [T] -) by stable expression of shRNA had decreased tumorigenesis and prolonged survival when compared to PAI-$1^{+/+}$ mice xenotransplanted with PAI-1 expressing tumor cells (H+/T+) (Fang et al., 2012). We examined these xenotransplanted tumors for the presence of TAM and observed a decrease in the number of F4/80 positive macrophages in H-/T- HT-1080 tumors compared to H+/T+ tumors (p=0.002) (Figure 1A). We also documented a decrease in arginase-positive (M2 marker) cells and an increase in iNOS-positive cells (M1 marker) in H-/T- tumors compared to H+/T+ tumors (p=0.042 and 0.026 respectively) (Figure 1B and C). Similar results were obtained with A549 tumors with a decrease in F4/80 positive macrophages (p=0.049), a decrease in arginase-positive cells and an increase in iNOS-positive cells in H-/T- tumors (p=0.033 and 0.038 respectively) (Figure 1D to F). Thus, absence of PAI-1 in tumors and host cells resulted in a decrease in the number of TAM and a switch in expression of polarization markers from M2 to M1.

PAI-1 expression is correlated with CD163 expression in human cancers

Supporting a link between PAI-1 and TAM polarization, an analysis of RNA-seq data from The Cancer Genome Atlas (TCGA) and gene expression array data from the Gene Expression Omnibus (GEO) database for PAI-1 and CD163 (an M2 marker) expression revealed a significant positive correlation between PAI-1 and CD163 expression in lung (r=0.70, p<0.01), colon (r=0.70, p<0.0001), prostate (r=0.83, p<0.0001), neuroblastoma (r=0.54, p<0.001), pancreatic (r=0.76, p<0.0001), medulloblastoma (r=0.65, p<0.001), ovarian (r=0.72, p<0.0001), glioblastoma (r=0.78, p<0.001) and bladder tumors (r=0.65, p<0.001) (Figure 1G and H).

PAI-1 promotes macrophage migration through its LRP1 interacting domain

Considering the known activity of PAI-1 on cell migration (Czekay et al., 2011), we first explored whether PAI-1 promoted the migration and recruitment of monocytes toward tumor cells. HT-1080 and A549 tumor cells stably transfected with a lentiviral vector expressing PAI-1 shRNA under the positive control of doxycycline (Tet ON) (HT-1080-Luc-shPAI1 and A549-Luc-shPAI1) were tested for their chemoattractant activity on human peripheral blood (PB) monocytes (Kubala and DeClerck, 2017). PAI-1 downregulation in doxycycline-treated HT-1080 and A549 cells (Figure 2A and B), decreased the migration of human monocytes toward the conditioned medium (CM) of the tumor cells by 61% and 65% respectively (Figure 2C and D). The chemoattractant activity of PAI-1 on monocytes was confirmed by migration experiments in the presence of recombinant (r)PAI-1 and mutant rPAI-1 R76E I91L which does not interact with LRP1 and rPAI-1 T333R A335R in which the mutation introduces a R-R cleavage site allowing uPA to cleave PAI-1, thus eliminating its anti-proteolytic activity (Figure 2E). rPAI-1 and rPAI-1 T333R A335R mutant promoted migration of PB monocytes whereas rPAI-1 R76E I91L mutant was inactive. Consistently, there was a loss of chemoattractant activity of rPAI-1 in the presence of the receptor associated protein (RAP), an inhibitor of PAI-1-LRP1 binding (Figure 2F and Figure S1). Thus, PAI-1 acts as a potent chemoattractant for monocytes through its ability to interact with the LRP1 receptor.

Author Manuscript Author Manuscript Author Manuscript Author Manuscript

PAI-1 polarizes macrophages towards an M2 phenotype through its uPA interacting domain

Our data also suggested that PAI-1 may affect macrophage polarization. In a series of no contact co-culture experiments with PB monocytes and HT-1080-Luc-shPAI-1 cells, we demonstrated an increase in CD163 expression in PB monocytes co-cultured with HT-1080 cells when compared to PB monocytes cultured alone. This increase was significantly reduced (by 46%, p=0.024) when PAI-1 expression was inhibited (by 70%) with doxycycline. In contrast, no decrease in CD163 expression occurred when doxycycline was added to the scrambled shRNA HT-1080 cells (Figure 3A). We validated these experiments in the presence of rPAI-1 and rPAI-1 mutants (Figure 3B). In four separate experiments, PB monocytes from different donors were treated with rPAI-1 and rPAI-1 mutants and examined for polarization. Despite a significant variability among each PB monocyte preparation, expression of CD163 consistently increased in all four preparations in the presence of rPAI-1 or rPAI-1 R76E I91L compared to untreated cells. In contrast, no increase in Median Fluorescence Intensity (MFI) CD163 was observed in the presence of rPAI-1 T333R A335R. Consistently, in the presence of rPAI-1 or rPAI-1 R76E I91L mutant, the expression of CD86 (an M1 marker) in PB monocytes decreased in all four preparations compared to untreated or rPAI-1 T333R A335R-treated PB monocytes. Low levels of CD80 expression in the presence of rPAI-1 and rPAI-1 R76E I91L but not in the presence of rPAI-1 T333R A335R were also observed. However, those levels were substantially lower than the level of CD163 expression, consistent with low levels of CD80 expression reported on M2 macrophages differentiated from human monocytes *in vitro* by treatment with M-CSF and IL-4 (Bayer et al., 2013; Raggi et al., 2017).

An analysis of the CM of PB monocytes treated with rPAI-1 and rPAI-1 R76E I91L indicated an induction of IL-10 and IL-12, with the levels of IL-10 being higher (average of 1,033 pg/mL and 1,863 pg/mL) than the levels of IL-12 (average of 285 pg/mL and 547 pg/mL) (Figure 3C). These changes in cytokines are consistent with an M2 polarization (Mantovani and Locati, 2013). Thus, these data indicate that the uPA interactive domain of PAI-1 is necessary for its activity on monocyte/macrophage polarization.

PAI-1-mediated macrophage polarization is IL-6- and STAT3-dependent

Interestingly, we also observed an induction of IL-6 in PB monocytes treated with rPAI-1 and rPAI-1 R76E I91L (average of 2,517 pg/mL and 2,299 pg/mL, respectively), but not with rPAI-1 T333R A335R (Figure 3D). The absence of endotoxin in the rPAI-1 preparations (Table S1) eliminated the possibility that IL-6 induction was due to lipopolysaccharides (LPS). Although IL-6 is not a typical M2 cytokine, it has been reported to induce and enhance the polarization of M2 macrophages (Fuster and Walsh, 2014). A gene expression analysis of PAI-1 and IL-6 in the GEO database revealed a positive correlation in lung (r=0.82, p<0.001), colon (r=0.8, p<0.0001), prostate (r=0.67, p<0.01), neuroblastoma (r=0.78, p<0.0001), ovarian (r=0.7, p<0.0001), pancreatic (r=0.6, p<0.01) medulloblastoma (r=0.29, p<0.05) and glioblastoma tumors (r=0.69, p<0.01) (Figure 3E). The analysis of the TCGA dataset of colon, breast and bladder cancer revealed a similar positive correlation in colon (r=0.6; p<0.01), breast (r=0.5; p=0.05), and bladder (r=0.58; p<0.001) cancers (Figure 3F).

Author Manuscript Author Manuscript Author Manuscript Author Manuscript

Treatment of PB monocytes with rPAI-1 induced IL-6 mRNA 2 h after treatment with a peak at 4 h, that preceded the release of IL-6 protein in the medium (4 h after treatment, with a peak at 8 h) (Figure 4A). The data are consistent with PAI-1 inducing the transcriptional expression of IL-6.

Macrophages express gp130 and gp80 IL-6 receptor proteins (Schoester et al., 1994) (Figure S2) and STAT3 is a known downstream signaling target of IL-6 (Zhong et al., 1994). An analysis of STAT3 activation in PB monocytes indicated an increase in phosphorylation (Y705) 8 h after treatment with rPAI-1 (Figure 4B), which corresponded to the peak of IL-6 protein in the medium. We further demonstrated an increase in STAT3 phosphorylation in PB monocytes co-cultured with doxycycline-regulated HT-1080-Luc-shPAI-1 upon removal of doxycycline from the co-cultures (Figure 4C). Consistent with this effect being mediated by PAI-1, STAT3 activation and IL-6 production were suppressed by the PAI-1 blocking antibody 8H9D4 (Debrock et al., 1997) (Figure 4D). STAT3 activation was not observed upon treatment of PB monocytes with rPAI-1 T333R A335R or upon heat denaturation of rPAI-1, but was seen in the presence of rPAI-1 or rPAI-1 R76E I91L (Figure 4E). We also demonstrated an absence of STAT3 phosphorylation in rPAI-1-treated PB monocytes pretreated with ruxolitinib (an inhibitor of JAK2/STAT3) or a function blocking antibody against IL-6R/gp80 (tocilizumab). Inhibition of STAT3 activation by these agents prevented the increase in CD163 in PB monocytes (Figure 4F and Figure S3). In two independent experiments in which PB monocytes were cultured with HT-1080 cells, we demonstrated that the addition of tocilizumab or ruxolitinib suppressed the increase in CD163 expression (tocilizumab p=0.01, ruxolitinib p=0.049) (Figure 4G). Altogether these data indicate that tumor-derived PAI-1 has a paracrine effect on monocyte/macrophage polarization by inducing an autocrine IL-6/STAT activation pathway.

IL-6/STAT3 activation by PAI-1 is p38MAPK-dependent

A Phospho-Kinase Array analysis of 30 proteins in PB monocytes exposed for 10 min to rPAI-1 or rPAI-1 T333R A335R as control, revealed an increase in phosphorylation of p38MAPK (3.0 fold), PRAS40 (2.3 fold), FAK (2.2 fold) and JNK½/3 (1.8 fold) with rPAI-1 over rPAI-1 T333R A335R (Figure 5A). The activation of p38MAPK in PB monocytes treated with rPAI-1 and in cultures of PB monocytes exposed to CM of HT-1080-Luc-shPAI1 cells in the absence of doxycycline was confirmed by western blot analysis (Figure 5B and C). Genetic suppression (siRNA) (Figure 5D) and pharmacological inhibition of p38MAPK by SB203580 (Figure 5E), a small molecule inhibitor of p38MAPK (Young et al., 1997) in rPAI-1-treated PB monocytes was associated with a decrease in STAT3 phosphorylation and pharmacological inhibition of p38MAPK in rPAI-1 treated PB monocytes suppressed IL-6 induction. Thus, p38MAPK activation is necessary for the induction of IL-6 and for IL-6-mediated STAT3 activation by rPAI-1.

Induction of IL-6 by p38MAPK is NF-κB -dependent

We then explored whether NF-κB, a known stimulator of IL-6 expression (Libermann and Baltimore, 1990), was involved in p38MAPK-mediated induction of IL-6 by rPAI-1.

Author Manuscript Author Manuscript Author Manuscript Author Manuscript

Exposure of PB monocytes to rPAI-1, but not rPAI-1 T333R A335R, increased the nuclear translocation of p65 (Figure 6A). Phosphorylation of p38MAPK, observed 2 min after treatment of PB monocytes with rPAI-1, was followed at 5 min by phosphorylation (Ser536) of the p65 subunit of NF-κB (Figure 6B). Consistent with NF-κB being downstream of p38MAPK activation, inhibition of p38MAPK by SB203580 blocked the nuclear translocation of p65 and its phosphorylation (Figure 6C) in rPAI-1-treated monocytes. Inhibition of p65 expression by siRNA also blocked STAT3 phosphorylation (Figure 6D), whereas pharmacological inhibition of NF-κB by the small molecule inhibitor BMS-345541 prevented STAT3 phosphorylation and IL-6 production in rPAI-1-treated PB monocytes (Figure 6E). Thus, altogether the data demonstrate that p38MAPK and its downstream effector NF-κB are responsible for the transcriptional activation of IL-6 by PAI-1.

Tumor-derived PAI-1 increases macrophage infiltration in xenotransplanted tumors.

To further document the contribution of PAI-1 to the recruitment and polarization of TAMs *in vivo*, a first experiment was performed in Rag1$^{-/-}$ PAI-1$^{-/-}$ mice (n=39) xenotransplanted with HT-1080-Luc-shPAI1 tumor cells (and shRNA scrambled controls, n=5). In this experiment the expression of tumor-derived PAI-1 in Rag1$^{-/-}$ PAI-1$^{-/-}$ mice xenotransplanted with HT-1080-Luc-shPAI1, after being suppressed by doxycycline for 30 days after implantation, was reestablished in one group and maintained in the other. Of 39 mice xenotransplanted with HT-1080-Luc-shPAI1, 12 mice did not develop tumors, which is consistent with a previously reported observation (Fang et al., 2012). Of the 27 tumor-bearing mice, 5 were sacrificed at day 30 and tumors analyzed for the presence of macrophages and PAI-1 expression. In 10 of the 22 remaining tumor-bearing mice, doxycycline was removed to allow PAI-1 expression, whereas it was maintained in the other 12 tumor-bearing mice. In these groups of mice, tumors were analyzed on day 37, 44 and 51 (Figure 7A). Mice xenotransplanted with scrambled control cells received doxycycline continuously and were sacrificed at day 44. This experiment revealed a high incidence (41%) of necrotic tumors in xenotransplanted mice in which the expression of PAI-1 was suppressed by doxycycline beyond 30 days (Figure 7B). In these necrotic tumors the microvessel density was generally lower, although the difference was not statistically significant (p=0.74) (Figure 7C). All HT-1080-LucshPAI1 tumors (n=27) were analyzed for the presence of F4/80^{+} macrophages by IHC and for PAI-1 expression (Figure 7D). The analysis of the HT-1080-Luc-shPAI1 tumors at day 30 (n=5) was not conclusive (not shown) but the analysis of tumors harvested at day 37, 44 and 51 indicated an overall strong direct correlation between the level of PAI-1 and the number of F4/80^{+} tumor infiltrating macrophages (rho=0.63, p=0.0016) (Figure 7E).

To allow a more in-depth analysis of TAM polarization and STAT3 activation in a larger number of tumors, a second experiment was done in which Rag1$^{-/-}$ PAI-1$^{-/-}$ mice (n=15) were xenotransplanted with HT-1080-Luc-shPAI1 tumor cells and Rag1$^{-/-}$ PAI-1$^{+/+}$ mice (n=15) xenotransplanted with HT-1080-Luc-scPAI1 tumor cells. In this experiment, half of the mice in each group received doxycycline for 35 days, when they were sacrificed and tumors analyzed (Figure 7F). One of the 8 Rag1$^{-/-}$ PAI-1$^{-/-}$ mice xenotransplanted with HT-1080-Luc-shPAI1 untreated with doxycycline (PAIKO noDOX) engrafted and 3 of the 7 Rag1$^{-/-}$ PAI-1$^{-/-}$ mice xenotransplanted with HT-1080-Luc-shPAI1 receiving doxycycline

Author Manuscript Author Manuscript Author Manuscript Author Manuscript

(PAIKO + DOX) did not engraft (Figure S4). An analysis of tumors at day 35 revealed a statistically significant decrease in pSTAT3 $^{+}$ F4/80^{+} macrophages and in CD206^{+} and CD163^{+} (M2 markers) cells associated with a statistically significant decrease in Arg^{+} cells and increase in iNOS $^{+}$ cells in the PAIKO +DOX group when compared to the other groups (PAIKO noDOX or PAIWT (Figure 7G–K). This experiment thus demonstrates that when tumor-derived PAI-1 is suppressed in the absence of host-derived PAI-1, there is not only inhibition of tumor formation but tumors that form are less infiltrated with M2 macrophages and there is less activation of STAT3 in macrophages, as predicted by our *in vitro* data. The levels of IL-6 and IL-10 in tumor lysates were not significantly different among the 4 groups in that experiment (Figure S5).

Because doxycycline used in these 2 experiments may have affected cytokine expression (Di Caprio et al., 2015), we performed a third experiment in Rag1$^{-/-}$ PAI-1$^{-/-}$ mice xenotransplanted with HT-1080-scPAI1 tumor cells (H-T+ n=15) and HT-1080-shPAI1 tumor cells (H-T- n=17) in which the downregulation of PAI-1 did not depend of doxycycline (Figure 7L). In this experiment we were able to demonstrate statistically significant lower levels of IL-6 and higher levels of IL-12 (M1) in tumors in which PAI-1 was knocked down by shRNA for 40 days (H-/T- group) (Figure 7M–N). The levels of IL-10 were also lower in this group but the difference was not statistically significant (Figure S6).

Within their limitations, these *in vivo* experiments however support our hypothesis and *in vitro* data demonstrating that PAI-1 promotes the migration and M2 polarization of TAM and an involvement of IL-6 and STAT3 in this function of PAI-1.

Discussion

In this manuscript we provide evidence for a pro-tumorigenic role of PAI-1 through a dual function on monocyte/macrophage migration and polarization. The pro-migratory function of PAI-1 demonstrated here is consistent with other studies showing that PAI-1 promotes smooth muscle cell migration through its interaction with the endocytic receptor LRP1 (Carmeliet et al., 1997) and the migration and phagocytic activity of microglial cells via a LRP1/JAK/STAT1 axis (Jeon et al., 2012). That PAI-1 coordinates Mac1-dependent macrophage migration has also been reported (Cao et al., 2006). Our observation that the N-terminal rPAI-1 R76E I91L mutant, not interacting with LRP1, did not stimulate human monocyte migration and that migration was blocked with RAP is consistent with an LRP1-mediated mechanism.

We clearly demonstrate that the effect of PAI-1 on macrophage polarization was mediated by a different mechanism than the one responsible for the pro-migratory function of PAI-1 as the rPAI-1 T333R A335R mutant did not promote macrophage polarization whereas it did stimulate migration. Thus, the dual function of PAI-1 on monocytes/macrophages is supported by two distinct domains, one affecting migration and the other polarization.

The observation that PAI-1 induced the expression of IL-6, a cytokine not typically associated with M2 polarization, led us to the demonstration of an autocrine IL-6/STAT3 pathway in macrophage polarization. IL-6 and STAT3 activation promotes polarization of

Author Manuscript Author Manuscript Author Manuscript Author Manuscript

macrophages towards the M2 phenotype in obese mice (Mauer et al., 2014) and in murine models of wound healing (Fernando et al., 2014) and cancer (Fu et al., 2017). The association between PAI-1 and IL-6 has been reported in multiple human conditions such as metabolic syndromes, obesity, diabetes, cardiovascular diseases, aging and cancer (Alberti et al., 2012; Van de Voorde et al., 2013; Vykoukal and Davies, 2011), however a cause-effect relation has never been previously explored.

Such cause-effect relation is clearly demonstrated by our data, as we provide evidence that the upregulation of IL-6 by PAI-1 and subsequent activation of STAT3 is p38MAPK- and NF-κB-dependent. p38MAPK has been reported to mediate IL-4-induced STAT-6 and Akt activation, leading to M2 polarization of mouse macrophages (Jimenez-Garcia et al., 2015). NF-κB is a known downstream target of p38MAPK and a known stimulator of IL-6 expression (Libermann and Baltimore, 1990), and contributes to the pro-tumorigenic polarization of TAM (Hagemann et al., 2008). Thus, we provide evidence that PAI-1 activates such a p38MAPK/NF-κB/IL-6 loop in a paracrine manner to promote M2 macrophage. Since IL-6 increases PAI-1 expression (Kruithof et al., 1997), activation of p38MAPK/NF-κB/IL-6 by PAI-1 could lead to a positive feedback loop in which increased IL-6 secretion results in more PAI-1 production.

The presence of an IL-6/STAT3 loop promoting macrophage M2 polarization by PAI-1 was also supported by our *in vivo* experiments. Because of the variability inherent to these experiments, the dependency on oral administration of doxycycline, and the overall lower number of tumors upon PAI-1 suppression, such demonstration required the completion of several experiments. Altogether however the data demonstrate that in tumors in which PAI-1 was downregulated by a doxycycline-dependent or independent mechanism, in addition to a decrease in the rate of tumor implantation and overall vascularization previously shown, there was a statistically significant decrease in M2 macrophages as demonstrated with several markers and in IL-6 and STAT3 activation in association with an increase in M1 macrophages.

Presently, the exact mechanism by which PAI-1 initiates p38MAPK-mediated signaling is unknown. It is conceivable that PAI-1 may enhance receptor-mediated signaling by inhibiting plasminogen activation into plasmin or by binding uPA, as reported previously in hippocampal neurons where plasmin or tPA have an inhibitory function on glutamate receptor mediated calcium release (Robinson et al., 2015). Alternatively, PAI-1 inhibition of plasmin generation via uPA inhibition may prevent the degradation of receptor or surface proteins that propagate a transmembrane signal. The possibility that PAI-1, independently from inhibiting uPA, directly activates p38MAPK and NF-κB by interacting at the cell surface with uPA/uPAR cannot be eliminated at this point. Such anti-protease-independent signaling activity of PAI-1 has been suggested to explain the pro-survival and proliferative functions of PAI-1 via Akt and ERK½ activation (Gramling and Church, 2010). As uPAR is a GPI-anchored protein that cannot induce signaling unless it interacts with other transmembrane receptors such as EGFR (Liu et al., 2002) or integrins (Smith and Marshall, 2010), we are presently exploring the presence of a potential signaling partner for the PAI-1/IL-6/STAT3 activation pathway.

Author Manuscript Author Manuscript Author Manuscript Author Manuscript

In summary, our data provide further evidence for a pro-tumorigenic role for PAI-1, pointing towards a possible targeting strategy for therapeutic purposes. Due to the importance of PAI-1 in cardiovascular diseases, lung fibrosis and cancer, several PAI-1 small molecule inhibitors have been developed and tested in different disease models. However, they have been ineffective so far in the clinic due either to their lack of activity against the stable, vitronectin-bound form of PAI-1 or to suboptimal pharmacokinetic properties (Placencio and DeClerck, 2015). To effectively target PAI-1 in cancer, better inhibitors adapted for chronic administration will have to be developed. Our data, providing an additional mechanism in support of the pro-tumorigenic function of PAI-1, should encourage such development.

STAR Methods

CONTACT FOR REAGENT AND RESOURCE SHARING

Further information and requests for resources and reagents should be directed to and will be fulfilled by the Lead Contact, Yves A. DeClerck (declerck@usc.edu).

EXPERIMENTAL MODEL AND SUBJECT DETAILS

Mice.—Rag1$^{-/-}$ PAI-1$^{-/-}$ and Rag1$^{-/-}$ PAI-1$^{+/+}$ immunodeficient mice were obtained by mating PAI-1-deficient mice (PAI-1$^{-/-}$) and their corresponding wild-type mice (PAI-1$^{+/+}$) on a mixed genetic background of 87% C57BL/6 and 13% 129 strain (Carmeliet et al., 1993) with *Rag-1*-deficient mice (*Rag-1*$^{-/-}$: B6; 129 s-Rag-1$^{tm/Mom}$/J) (Bajou et al., 2008). 6–8 week old female and male mice were used for *in vivo* experiments. Littermates of both sexes were randomly assigned to experimental groups and the equal number of both sexes was allocated in each group. Animals used in experiments were healthy and not involved in previous procedures. Mice were kept in the animal care facility, in pressure-controlled rooms solely dedicated to the housing of immunodeficient mice at a maximum of 5 mice per cage. The animal care facility is accredited by AAALAC and received its most recent 3 year accreditation in 2017. Animal experiments were performed in accordance with a protocol approved by the Institutional Animal Care and Use Committee at CHLA (Protocol #41–14 approved on November 7, 2014).

Cell lines.—The HT-1080 fibrosarcoma cancer cell line derived from male patient was purchased from ATCC in Nov. 2014. A549 epithelial lung cancer cell line derived from male patient (Lieber et al., 1976) was obtained from H. Fang (Fang et al., 2012). Cell lines were authenticated by short tandem repeat profile genotyping analysis in March 2018. Mycoplasma testing was monthly performed using MycoAlert Mycoplasma Detection Kit (Lonza). Human PB monocytes were used fresh after isolation from the excess material (discarded filters) of normal, adult, blood platelet donors from CHLA Blood Bank, and approved in the Human Material Protocol CCI 08–00208. Donors include different ethnic backgrounds, men and women and are anonymous. Cells were cultured in Roswell Park Memorial Institute-1640 medium (RPMI-1640; Gibco) or Dulbecco's Modified Eagle's Medium (DMEM; Gibco) containing 10% tetracycline (tet)-free FBS (Omega Scientific) and 1% (v/v) penicillin/streptomycin (100 units/mL of penicillin, 100 μg/mL of streptomycin; Gibco) and incubated at 37°C and 5% CO_2.

Author Manuscript Author Manuscript Author Manuscript Author Manuscript

METHOD DETAILS

Reagents.—The antibodies used for western blotting, flow cytometry and immunohistochemistry are listed in the Key Resources Table. rPAI-1, rPAI-1 T333R A335R, rPAI-1 R76E I91L and RAP proteins were purchased from Molecular Innovations and used in experiments at a final concentration of 40 nM and 100 nM. Recombinant proteins tested negative by Endolisa assay (Hyglos) for the presence of endotoxin (LPS) (< 0.05 EU/μg of protein) (Table S1). Doxycyline (Sigma Aldrich) was dissolved in water at 10 mg/mL, filter sterilized (0.2 μm) and kept at −20°C in darkness. Actemra (Tocilizumab) was purchased from Genentech. SB203580 was purchased from Cell Signaling. BMS-345541 was purchased from Sigma-Aldrich. Ruxolitinib was purchased from Selleckchem. Inhibitors were dissolved in DMSO at a final 10 mM stock concentration.

Isolation of human monocytes.—The detailed method has been previously published (Kubala and DeClerck, 2017). In brief, white blood cells concentrated in a leukocyte filter obtained from healthy platelet donors were diluted to 90 mL with 1% (v/v) tet-free FBS (FBS-PBS) and layered over 15 mL of Histopaque (Sigma). After centrifugation at 400 g with break set on 0, the upper layer was removed and the mononuclear cell layer was transferred to a new tube and washed 3 times with PBS containing 1% FBS-PBS by centrifugation at 120 g to remove platelets. Cells were counted and T cells, NK cells, neutrophils, B cells, granulocytes and erythrocytes were removed using a cocktail of antibodies (anti-CD2, CD3, CD16, CD19, CD20, CD56, CD66b, CD123, glycophorin A) with an EasySep kit (StemCell) according to the manufacturer's protocol. Negatively selected PB monocytes were then cultured in RPMI medium (Gibco) supplemented with 10% (v/v) tet-free FBS and 1% (v/v) Pen/Strep.

Boyden chamber migration assay.—Boyden chamber migration assay was performed as described before (Kubala and DeClerck, 2017). Porous membrane size inserts (8 μm; Transwell Corning) were incubated in 1% (w/v) bovine serum albumin (BSA) overnight and washed with PBS. Cancer cells (40,000) were plated in a 24-well plate in triplicate. The next day, 8000 PB monocytes in RPMI medium containing 10% Tet-free FBS and 1% Pen/Strep were plated on the membrane filters in triplicate, and incubated at 37°C and 5% CO_2. After 48 h, filters were collected, the inner surface was swiped with a cotton-tipped applicator and filters were stained using a Hema 3 stain kit (Protocol). Monocytes were counted (9 fields per filter) using a 20x light microscope objective, averaged per field and multiplied by the factor of 50 to obtain a number of monocytes per filter. The average of technical triplicates was calculated.

HT-1080- and A549-Luc-shPAI1 cell lines.—Anti PAI-1 shRNA sequences were cloned into the pLKO-Tet-On vector (Addgene #21915) as described (Wee et al., 2008; Wiederschain et al., 2009). To produce the virus, human embryonic kidney HEK293 cells were transformed with pLKO-shRNAPAI1, psPAX2, and pMD2.G vectors, which were gifts from Didier Trono lab, using Lipofectamine 2000 according to the manufacturer's instructions, and were induced the next day with sodium butyrate for 8 h. After 48 h, virus-containing medium was collected and added to the HT-1080- Luciferase and A549-Luciferase cells for overnight incubation. In the morning, the medium was changed to

Author Manuscript Author Manuscript Author Manuscript Author Manuscript

DMEM 10% (v/v) tet-free FBS. After 48 h, medium was changed and Puromycin (1 μg/mL) and Geneticin (100 μg/mL) were added and maintained for two weeks for the negative selection of resistant clones.

HT-1080-shPAI1 and HT-1080-scPAI1 cell lines.—HT-1080 cell line stably expressing shRNA against PAI-1 and scrambled control was developed as described previously (Fang et al., 2012).

Elisa.—Cell culture media from the *in vitro* experiments were analyzed for the expression levels of human IL-6, IL-10 and IL-12 cytokines using DuoSet Elisa Assays (R&D) according to the manufacturer's protocol.

Fluorescence-Activated Cell Sorting.—Cells were collected using a PBS-based dissociation buffer (Gibco) and washed twice with FACS buffer (PBS, 0.1% (v/w) NaN_3, 0.2% (v/w) BSA). Five μL of human TruStain FcX (BioLegend) receptor blocking solution was added to all samples, and after 15 min the antibodies and isotype-matched control antibodies (Biolegend) were added to the samples and incubated in darkness for 45 min. Samples were washed twice with FACS buffer and after adding 500 ng/mL of 4',6-diamidino-2-phenylindole (DAPI) filtered through 40 μm mesh. Median Fluorescence Intensity (MFI) was calculated as the median fluorescence of viable $CD14^+$ cells stained with the specific antibody divided by median fluorescence of viable $CD14^+$ cells stained with the isotype matched control.

Preparation of conditioned medium.—HT-1080-Luc-shPAI1 and scramble control cells were seeded in 152 cm^2 dishes and grown in RPMI 10% (v/v) tet-free FBS medium in absence or presence of 1 μg/mL doxycycline for 72 h. The medium was collected, centrifuged to remove dead cells, filtered through a 0.45 μm filter and stored at −80°C.

PAI-1 inhibition.—100 nM rPAI-1 was preincubated with 5 μg/mL of PAI-1 blocking antibody (MA-8H9D4, Molecular Innovations) and with 5 μg/mL isotype antibody as a control (LEAF^{tm} Purified Mouse IgG1 K isotype cntr, Biolegend). PB monocytes were treated with pre-incubated proteins for 5 h and analyzed for STAT3 phosphorylation by western blot and IL-6 expression in the medium by ELISA.

Western blotting.—Proteins (30 μg) were loaded onto a 4–15% gradient pre-cast gel (Bio-RAD), transferred onto a nitrocellulose membrane via semi-dry transfer and blocked for 1 h with Odyssey blocking buffer (LI-COR). Primary antibodies at 1:1000 dilution were incubated overnight at 4°C with agitation. Secondary antibodies conjugated with fluorochromes - goat anti-rabbit 800CW and secondary donkey anti-mouse 680LT (1:15000 dilution; LI-COR) were incubated for 2 h at room temperature (RT) and immune complexes were detected using the Odyssey Infrared Imaging System (LI-COR). Pixel density measurements for calculation of the protein/actin or protein/tubulin ratio were obtained using the software of LI-COR Biosciences.

Proteome Profiler Human Phospho-Kinase Array.—PB monocytes exposed for 10 min to rPAI-1 and rPAI-1 T333R A335R were lysed and examined for the phosphorylation

Author Manuscript Author Manuscript Author Manuscript Author Manuscript

of 30 kinases using a Human Phospho-Kinase Array (R&D System) according to the manufacturer's instructions. Briefly, membranes were incubated with cell lysates (200 μg), followed by washing and incubation with a cocktail of biotinylated antibodies overnight at 4°C. Membranes were then washed three times and incubated in the presence of streptavidin-horseradish peroxidase (HRP) for 30 min at RT, and the presence of immunocomplexes was then detected by staining with the 3,3'-diaminobenzidine (DAB) chromogen. Membranes were scanned using the Odyssey Infrared Imaging System (LI-COR) and pixel density measurements were obtained using the software of LI-COR Biosciences.

Immunofluorescence (IF).—PB monocytes were seeded on glass coverslips covered with poly-L-Lysine and cultured overnight at 37°C and 5% CO_2. Cells were then fixed in 4% (w/v) paraformaldehyde in PBS at RT for 10 min, washed with PBS, permeabilized with 0.1% (v/v) Triton X-100 in PBS for 5 min at RT, blocked with 15% (v/v) FBS in PBS at RT for 30 min and incubated for 1 h at 37°C in the presence of primary antibody against NF-κB (1:400 dilution; Cell Signaling). After washing with 0.1% Triton X-100 twice for 5 min, slides were incubated for 45 min at RT with secondary antibody conjugated with DyLight® 488 (at 1:300 dilution; Vector Labs). Following six washes with 0.1% Triton X-100, cells were embedded in VectaShield mounting medium with 4,6-diamidino-2-phenylindole (DAPI; Vector Laboratories). Fluorescence images were captured using an LSM 710 confocal system. Blue nuclei were counted using FIJI ImageJ software (Schindelin et al., 2012). Cell nucleus objects were thresholded in the blue channel. Positive green nuclei were counted manually in technical triplicate.

TCGA RNA-seq data analysis.—TCGA RNA-seq data was retrieved using TCGA assembler (Zhu et al., 2014). The normalized transcript count data was used to calculate the correlation coefficient in two-group analysis as indicated in the figures. Scatter plot of normalized count was generated in SigmaXL. A two-sided t-test was used to obtain the p values and significance of difference in two groups.

Gene array analysis.—For gene expression meta-analysis, patient microarray expression data corresponding to colon cancer (GSE33114; GSE9452; GSE18088; GSE14333; GSE17538; GSE4183; GSE2109), neuroblastoma (GSE15583; GSE16476; GSE16237; GSE16254; GSE3446), lung cancer (GSE2109; GSE43580; GSE19188; GSE63074; GSE2109), breast cancer (GSE14018; GSE12276), prostate cancer (GSE2109; E-TABM-90; GSE6956; GSE21034), pancreatic cancer (GSE16515; GSE32676; GSE32676; E-MEXP-950), ovarian cancer (GSE12172; GSE40595; GSE9891; GSE26193), glioblastoma (GSE36245; GSE7696; GSE4271; GSE18015), medulloblastoma (GSE67851; GSE74195; GSE7578; GSE49243) were obtained from the GEO database. The signal intensities were extracted using Robust Multi-array Average (RMA) algorithm and data was quintile-normalized. The correlation of expression between two genes was calculated using the Pearson correlation. A two-sided t-test was used to obtain the p values and significance of difference in two groups.

Author Manuscript Author Manuscript Author Manuscript Author Manuscript

RT-PCR.—Quantitative RT-PCR was performed using Taqman assays (Thermo Fisher Scientific) on a 7900 HT Fast Real-Time PCR (Applied Biosystems) system. cDNA was generated from 300 ng of RNA using reverse transcription using SuperScript® III First-Strand Synthesis System (Invitrogen). Triplicate aliquots from each sample were tested for each gene, and average threshold cycle (Ct) numbers were calculated. Gene expression levels were normalized against GAPDH and expressed as ΔCt. The data was analyzed using $2^{-\Delta Ct}$ method. Catalog numbers of TaqMan Gene Expression Assays (Applied Biosystems) used to amplify cDNAs are listed in the Key Resources Table.

***In vivo* experiments.—**HT-1080-Luc-shPAI1 and HT-1080-Luc-scPAI1 cells (4×10^6) were injected in the right flank of Rag1$^{-/-}$ PAI-1$^{-/-}$ and Rag1$^{-/-}$ PAI-1$^{+/+}$ mice. Mice were euthanized with O_2/CO_2 at indicated times days or when tumors reached 1,500 mm^3, or when animals were in distress. When indicated, mice received doxycycline (2 mg/mL) in drinking water.

In other experiments, Rag1$^{-/-}$ PAI-1$^{-/-}$ mice were injected in the right flank with HT-1080-shPAI1 and HT-1080-scPAI1 cells (4×10^6). Tumors were harvested and separated in segments for fixation in formalin and for homogenization in lysis buffer (Thermo Fisher Scientific). The protein concentration in the lysates after removal of the debris was measured by the BCA Assay. Tumor lysates were analyzed for expression levels of mouse cytokines using the DuoSet Elisa Assays (R&D) according to the manufacturer's protocol. To assess the expression of PAI-1 in the tumors, tumor tissues were homogenized in lysis buffer (tris buffered saline, 1% Triton X-100, protease inhibitors (Thermo Fisher Scientific)).

Immunohistochemistry.—Antigen retrieval for arginase and iNOS and CD206 was performed by heating the slides with antigen unmasking solution, low pH (Vector Laboratories; 1:100). For F4/80 stain, antigen retrieval was performed by incubating slides with Proteinase K (at 20 μg/mL final concentration). Slides were incubated with Bloxall solution (Vector Laboratories) and blocked in 5% (v/v) goat serum in PBS. Slides were then incubated overnight at 4°C with antibodies against iNOS (1:100; Abcam), arginase (1:50; Santa Cruz) and F4/80 (at 1:250; Abcam). Slides were washed with PBS and incubated with the appropriate biotinylated secondary antibody and incubated with the Vectastain ABC immunoperoxidase detection system according to manufacturer's instructions (Vector Laboratories). Slides were then stained with DAB chromogen, counterstained with methyl green and mounted using xylene based medium. Positive cells were counted in five random fields at 20x magnification in five sections for each tumor. For dual pSTAT3 and F4/80 stain, 5 μm sections were baked at 70°C for 30 min and dewaxed with the Gemini Auto Stainer (Thermo Scientific). Antigen retrieval was performed at 125°C for 90 sec in pH 9.0 (CC1 buffer, Ventana). Slides were incubated for 30 min with pSTAT3 rabbit mAb (at 1:100 dilution; Cell Signaling). Further Bond Polymer Refine detection kit was used according to the manufacturer's settings. After DAB, the antigen retrieval was performed at 125°C for 90 sec in pH 6.0 (ER1 retrieval buffer, Leica). Slides were incubated for 30 min with F4/80 rat mAb (at 1:300 dilution; Abcam) followed by adding the rabbit anti-rat IgG secondary antibody (at 1:1000 dilution) for 30 min. Further Bond Polymer Refine Red detection kit was used according to the manufacturers' settings.

Author Manuscript Author Manuscript Author Manuscript Author Manuscript

Immunofluorescence CD31.—Tumors extracted from mice were embedded in paraffin, cut on a microtome instrument (Leica) in 5 μm-thick sections that were then placed on positively charged microscope slides (VWR). Slides were de-paraffinized in xylene and rehydrated in a series of ethanol solutions (100%, 95%, 70%, 50%, water). Sections were permeabilized by incubating with PBS-T (PBS, 1% Triton X-100) for 15 min at RT and rinsed with water. Antigen retrieval was performed by incubating the slides for 13 min at RT with Proteinase K (at 20 μg/mL final concentration). Slides were washed with PBS 3 × 3 min and incubated with blocking buffer (5% (v/v) goat serum, 1% BSA, 0.5% Tween20 in PBS) for 60 min at RT. Slides were then incubated overnight at 4°C with a rat antibody against CD31 (at 1:100 dilution; Abcam) in a humid chamber. Slides were washed with PBS-T 3 × 10 min and with PBS for 5 min and incubated with the anti-rat secondary antibody conjugated with Cy3 fluorochrome (at 1:300 dilution; Jackson ImmunoResearch) for 2 h. After washing with PBS-T 3 × 10 min and PBS for 5 min, slides were mounted using VectaShield mounting medium with DAPI (Vector Laboratories).

Microscopy and image analysis.—Images were acquired on a DMI6000B microscope equipped with a 20×/0.7 HC PLAN APO Ph2 objective lens and a DFC290 color CCD camera (Leica Microsystems, Buffalo Grove, IL) for IHC and an ORCA-Flash4.0 LT sCMOS camera (Hamamatsu Photonics, Bridgewater, NJ) for IF. Area covered by red stain was quantified automatically using FIJI ImageJ software (Schindelin et al., 2012) with custom macros that performed, for IHC images: shading correction, background subtraction, color deconvolution with custom color vectors, auto threshold with the Yen algorithm, and median filtering (radius 1); or, for IF images: color thresholding with a custom color definition and median filtering (radius 4). IF images with high background were color-thresholded manually and not median-filtered before quantification.

Quantification and Statistical Analysis

Tests of difference in means between groups comprising independent, non-matched observations were based on the two-sample t-test or analysis of variance. Tests of difference in means between groups comprising independent, non-matched observations were based on the two-sample t-test or analysis of variance, as appropriate. Tests of mean of ratios of expression values compared to unity were based on a one-sample t-test. Test of significance of correlation coefficients were Student's t-tests for correlations. All p-values are two sided. $p < 0.05$ is generally considered significant. P-values presented are not adjusted for multiple comparisons (Rothman, 1990). Statistical computation was performed using Stata (StataCorp. 2015. Stata Statistical Software: Release 14. College Station, TX: StataCorp LP) and Graphpad Prism version 6.00 for Windows (GraphPad Software, La Jolla, California USA, www.graphpad.com). All data has been included in analysis.

Supplementary Material

Refer to Web version on PubMed Central for supplementary material.

Author Manuscript Author Manuscript Author Manuscript Author Manuscript

Acknowledgements

The authors would like to acknowledge J. Rosenberg for proofreading the manuscript and Dr. Martine Torres for editorial assistance. This work was supported by the US Department of Health and Human Services/NIH with a grant to YA DeClerck (grant 5R01 CA129377) and the TJ Martell Foundation. MH Kubala is the recipient of a Research Career Development Fellowship of The Saban Research Institute at CHLA.

References

Alberti C, Pinciroli P, Valeri B, Ferri R, Ditto A, Umezawa K, Sensi M, Canevari S, and Tomassetti A (2012). Ligand-dependent EGFR activation induces the co-expression of IL-6 and PAI-1 via the NFkB pathway in advanced-stage epithelial ovarian cancer. Oncogene 31, 4139–4149. [PubMed: 22158046]

Bajou K, Masson V, Gerard RD, Schmitt PM, Albert V, Praus M, Lund LR, Frandsen TL, Brunner N, Dano K, et al. (2001). The plasminogen activator inhibitor PAI-1 controls in vivo tumor vascularization by interaction with proteases, not vitronectin. Implications for antiangiogenic strategies. J Cell Biol 152, 777–784. [PubMed: 11266468]

Bajou K, Peng H, Laug WE, Maillard C, Noel A, Foidart JM, Martial JA, and DeClerck YA (2008). Plasminogen activator inhibitor-1 protects endothelial cells from FasL-mediated apoptosis. Cancer Cell 14, 324–334. [PubMed: 18835034]

Bayer C, Varani S, Wang L, Walther P, Zhou S, Straschewski S, Bachem M, Soderberg-Naucler C, Mertens T, and Frascaroli G (2013). Human cytomegalovirus infection of M1 and M2 macrophages triggers inflammation and autologous T-cell proliferation. J Virol 87, 67–79. [PubMed: 23055571]

Cao C, Lawrence DA, Li Y, Von Arnim CA, Herz J, Su EJ, Makarova A, Hyman BT, Strickland DK, and Zhang L (2006). Endocytic receptor LRP together with tPA and PAI-1 coordinates Mac-1-dependent macrophage migration. EMBO J 25, 1860–1870. [PubMed: 16601674]

Carmeliet P, Moons L, Lijnen R, Janssens S, Lupu F, Collen D, and Gerard RD (1997). Inhibitory role of plasminogen activator inhibitor-1 in arterial wound healing and neointima formation: a gene targeting and gene transfer study in mice. Circulation 96, 3180–3191. [PubMed: 9386191]

Carmeliet P, Stassen JM, Schoonjans L, Ream B, van den Oord JJ, De Mol M, Mulligan RC, and Collen D (1993). Plasminogen activator inhibitor-1 gene-deficient mice. II. Effects on hemostasis, thrombosis, and thrombolysis. J Clin Invest 92, 2756–2760. [PubMed: 8254029]

Czekay RP, Wilkins-Port CE, Higgins SP, Freytag J, Overstreet JM, Klein RM, Higgins CE, Samarakoon R, and Higgins PJ (2011). PAI-1: An Integrator of Cell Signaling and Migration. Int J Cell Biol 2011, 562481. [PubMed: 21837240]

Debrock S, Sironi L, and Declerck PJ (1997). Cloning of a single-chain variable fragment (scFv) switching active plasminogen activator inhibitor-1 to substrate. Gene 189, 83–88. [PubMed: 9161416]

Di Caprio R, Lembo S, Di Costanzo L, Balato A, and Monfrecola G (2015). Anti-inflammatory properties of low and high doxycycline doses: an in vitro study. Mediators Inflamm 2015, 329418. [PubMed: 25977597]

Duffy MJ, O'Donovan N, McDermott E, and Crown J (2016). Validated biomarkers: The key to precision treatment in patients with breast cancer. Breast 29, 192–201. [PubMed: 27521224]

Fang H, Placencio VR, and DeClerck YA (2012). Protumorigenic activity of plasminogen activator inhibitor-1 through an antiapoptotic function. J Natl Cancer Inst 104, 1470–1484. [PubMed: 22984202]

Fernando MR, Reyes JL, Iannuzzi J, Leung G, and McKay DM (2014). The pro-inflammatory cytokine, interleukin-6, enhances the polarization of alternatively activated macrophages. PLoS One 9, e94188. [PubMed: 24736635]

Fu XL, Duan W, Su CY, Mao FY, Lv YP, Teng YS, Yu PW, Zhuang Y, and Zhao YL (2017). Interleukin 6 induces M2 macrophage differentiation by STAT3 activation that correlates with gastric cancer progression. Cancer Immunol Immunother.

Fuster JJ, and Walsh K (2014). The good, the bad, and the ugly of interleukin-6 signaling. EMBO J 33, 1425–1427. [PubMed: 24850773]

Author Manuscript Author Manuscript Author Manuscript Author Manuscript

Gramling MW, and Church FC (2010). Plasminogen activator inhibitor-1 is an aggregate response factor with pleiotropic effects on cell signaling in vascular disease and the tumor microenvironment. Thromb Res 125, 377–381. [PubMed: 20079523]

Hagemann T, Lawrence T, McNeish I, Charles KA, Kulbe H, Thompson RG, Robinson SC, and Balkwill FR (2008). "Re-educating" tumor-associated macrophages by targeting NF-kappaB. J Exp Med 205, 1261–1268. [PubMed: 18490490]

Huntington JA, Read RJ, and Carrell RW (2000). Structure of a serpin-protease complex shows inhibition by deformation. Nature 407, 923–926. [PubMed: 11057674]

Isogai C, Laug WE, Shimada H, Declerck PJ, Stins MF, Durden DL, Erdreich-Epstein A, and DeClerck YA (2001). Plasminogen activator inhibitor-1 promotes angiogenesis by stimulating endothelial cell migration toward fibronectin. Cancer Res 61, 5587–5594. [PubMed: 11454712]

Jeon H, Kim JH, Kim JH, Lee WH, Lee MS, and Suk K (2012). Plasminogen activator inhibitor type 1 regulates microglial motility and phagocytic activity. J Neuroinflammation 9, 149. [PubMed: 22747686]

Jimenez-Garcia L, Herranz S, Luque A, and Hortelano S (2015). Critical role of p38 MAPK in IL-4-induced alternative activation of peritoneal macrophages. Eur J Immunol 45, 273–286. [PubMed: 25328047]

Kruithof EK, Mestries JC, Gascon MP, and Ythier A (1997). The coagulation and fibrinolytic responses of baboons after in vivo thrombin generation--effect of interleukin 6. Thromb Haemost 77, 905–910. [PubMed: 9184401]

Kubala MH, and DeClerck YA (2017). Conditional Knockdown of Gene Expression in Cancer Cell Lines to Study the Recruitment of Monocytes/Macrophages to the Tumor Microenvironment. J Vis Exp 129, e56333.

Lawrence DA, Olson ST, Muhammad S, Day DE, Kvassman JO, Ginsburg D, and Shore JD (2000). Partitioning of serpin-proteinase reactions between stable inhibition and substrate cleavage is regulated by the rate of serpin reactive center loop insertion into beta-sheet A. J Biol Chem 275, 5839–5844. [PubMed: 10681574]

Libermann TA, and Baltimore D (1990). Activation of interleukin-6 gene expression through the NF-kappa B transcription factor. Mol Cell Biol 10, 2327–2334. [PubMed: 2183031]

Lieber M, Smith B, Szakal A, Nelson-Rees W, and Todaro G (1976). A continuous tumor-cell line from a human lung carcinoma with properties of type II alveolar epithelial cells. Int J Cancer 17, 62–70. [PubMed: 175022]

Liu D, Aguirre Ghiso J, Estrada Y, and Ossowski L (2002). EGFR is a transducer of the urokinase receptor initiated signal that is required for in vivo growth of a human carcinoma. Cancer Cell 1, 445–457. [PubMed: 12124174]

Mantovani A, and Locati M (2013). Tumor-associated macrophages as a paradigm of macrophage plasticity, diversity, and polarization: lessons and open questions. Arteriosclerosis, thrombosis, and vascular biology 33, 1478–1483.

Mauer J, Chaurasia B, Goldau J, Vogt MC, Ruud J, Nguyen KD, Theurich S, Hausen AC, Schmitz J, Bronneke HS, et al. (2014). Signaling by IL-6 promotes alternative activation of macrophages to limit endotoxemia and obesity-associated resistance to insulin. Nat Immunol 15, 423–430. [PubMed: 24681566]

Mengele K, Napieralski R, Magdolen V, Reuning U, Gkazepis A, Sweep F, Brunner N, Foekens J, Harbeck N, and Schmitt M (2010). Characteristics of the level-of-evidence-1 disease forecast cancer biomarkers uPA and its inhibitor PAI-1. Expert Rev Mol Diagn 10, 947–962. [PubMed: 20964613]

Murray PJ, Allen JE, Biswas SK, Fisher EA, Gilroy DW, Goerdt S, Gordon S, Hamilton JA, Ivashkiv LB, Lawrence T, et al. (2014). Macrophage activation and polarization: nomenclature and experimental guidelines. Immunity 41, 14–20. [PubMed: 25035950]

Oda T, Jung YO, Kim HS, Cai X, Lopez-Guisa JM, Ikeda Y, and Eddy AA (2001). PAI-1 deficiency attenuates the fibrogenic response to ureteral obstruction. Kidney Int 60, 587–596. [PubMed: 11473641]

Placencio VR, and DeClerck YA (2015). Plasminogen Activator Inhibitor-1 in Cancer: Rationale and Insight for Future Therapeutic Testing. Cancer Res 75, 2969–2974. [PubMed: 26180080]

Author Manuscript Author Manuscript Author Manuscript Author Manuscript

Raggi F, Pelassa S, Pierobon D, Penco F, Gattorno M, Novelli F, Eva A, Varesio L, Giovarelli M, and Bosco MC (2017). Regulation of Human Macrophage M1–M2 Polarization Balance by Hypoxia and the Triggering Receptor Expressed on Myeloid Cells-1. Front Immunol 8, 1097. [PubMed: 28936211]

Robinson SD, Lee TW, Christie DL, and Birch NP (2015). Tissue plasminogen activator inhibits NMDA-receptor-mediated increases in calcium levels in cultured hippocampal neurons. Front Cell Neurosci 9, 404. [PubMed: 26500501]

Rothman KJ (1990). No adjustments are needed for multiple comparisons. Epidemiology 1, 43–46. [PubMed: 2081237]

Schindelin J, Arganda-Carreras I, Frise E, Kaynig V, Longair M, Pietzsch T, Preibisch S, Rueden C, Saalfeld S, Schmid B, et al. (2012). Fiji: an open-source platform for biological-image analysis. Nat Methods 9, 676–682. [PubMed: 22743772]

Schoester M, Heinrich PC, and Graeve L (1994). Regulation of interleukin-6 receptor expression by interleukin-6 in human monocytes--a re-examination. FEBS Lett 345, 131–134. [PubMed: 8200444]

Seiffert D, Ciambrone G, Wagner NV, Binder BR, and Loskutoff DJ (1994). The somatomedin B domain of vitronectin. Structural requirements for the binding and stabilization of active type 1 plasminogen activator inhibitor. J Biol Chem 269, 2659–2666. [PubMed: 7507927]

Smith HW, and Marshall CJ (2010). Regulation of cell signalling by uPAR. Nat Rev Mol Cell Biol 11, 23–36. [PubMed: 20027185]

Stefansson S, Muhammad S, Cheng XF, Battey FD, Strickland DK, and Lawrence DA (1998). Plasminogen activator inhibitor-1 contains a cryptic high affinity binding site for the low density lipoprotein receptor-related protein. J Biol Chem 273, 6358–6366. [PubMed: 9497365]

Van de Voorde J, Pauwels B, Boydens C, and Decaluwe K (2013). Adipocytokines in relation to cardiovascular disease. Metabolism 62, 1513–1521. [PubMed: 23866981]

Vykoukal D, and Davies MG (2011). Vascular biology of metabolic syndrome. J Vasc Surg 54, 819–831. [PubMed: 21439758]

Wee S, Wiederschain D, Maira SM, Loo A, Miller C, deBeaumont R, Stegmeier F, Yao YM, and Lengauer C (2008). PTEN-deficient cancers depend on PIK3CB. Proc Natl Acad Sci U S A 105, 13057–13062. [PubMed: 18755892]

Wiederschain D, Wee S, Chen L, Loo A, Yang G, Huang A, Chen Y, Caponigro G, Yao YM, Lengauer C, et al. (2009). Single-vector inducible lentiviral RNAi system for oncology target validation. Cell Cycle 8, 498–504. [PubMed: 19177017]

Xu X, Wang H, Wang Z, and Xiao W (2009). Plasminogen activator inhibitor-1 promotes inflammatory process induced by cigarette smoke extraction or lipopolysaccharides in alveolar epithelial cells. Exp Lung Res 35, 795–805. [PubMed: 19916862]

Young PR, McLaughlin MM, Kumar S, Kassis S, Doyle ML, McNulty D, Gallagher TF, Fisher S, McDonnell PC, Carr SA, et al. (1997). Pyridinyl imidazole inhibitors of p38 mitogen-activated protein kinase bind in the ATP site. J Biol Chem 272, 12116–12121. [PubMed: 9115281]

Zhong Z, Wen Z, and Darnell JE Jr. (1994). Stat3: a STAT family member activated by tyrosine phosphorylation in response to epidermal growth factor and interleukin-6. Science 264, 95–98. [PubMed: 8140422]

Zhu Y, Qiu P, and Ji Y (2014). TCGA-assembler: open-source software for retrieving and processing TCGA data. Nat Methods 11, 599–600. [PubMed: 24874569]

Author Manuscript Author Manuscript Author Manuscript Author Manuscript

Significance

The serine protease inhibitor plasminogen activator inhibitor-1 is overexpressed in most cancers and its expression positively correlates with more aggressive disease, lower response to therapy and poor clinical outcome, indicating a paradoxical pro-tumorigenic function. Here, we report a mechanism explaining such pro-tumorigenic function through PAI-1 activity on the recruitment and polarization toward a pro-tumorigenic phenotype of tumor-associated macrophages (TAM). The data bring further insight to the concept that targeting PAI-1 should be considered in cancer therapy.

Author Manuscript
Author Manuscript
Author Manuscript
Author Manuscript

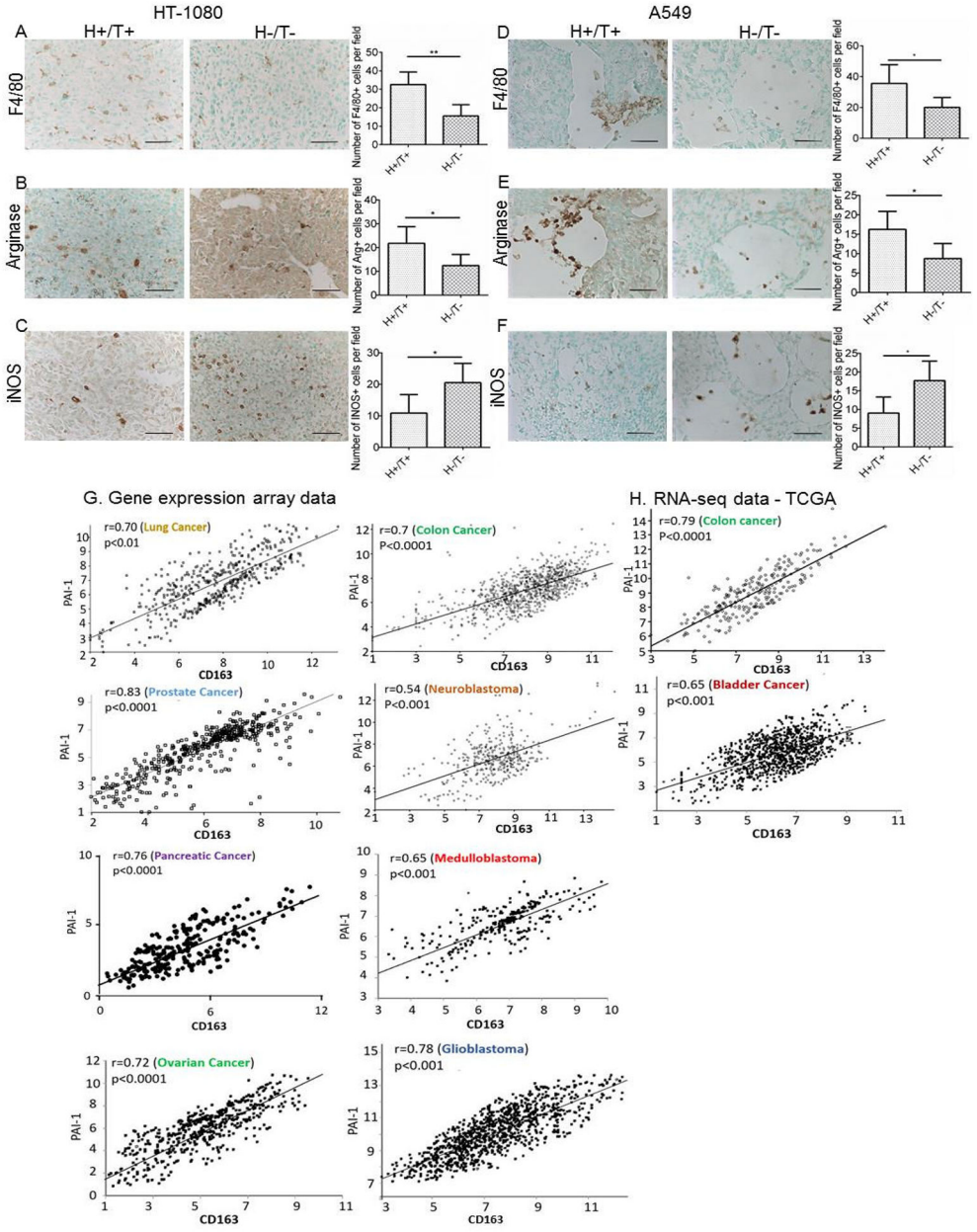

Figure 1. Decrease in macrophage infiltration and arginase expression, and increase in iNOS expression in the absence of host- and tumor-derived PAI-1 in HT-1080 and A549 tumors.

A-F. HT-1080 and A549 cells stably expressing PAI-1 shRNA (T−) or scramble control shRNA (T+) were injected subcutaneously into the right flank of Rag-$1^{-/-}$ PAI-$1^{-/-}$ mice (H-) and Rag-$1^{-/-}$ PAI-$1^{+/+}$ mice (H+), respectively. Representative immunohistochemical staining of HT-1080 (A-C) and A549 (D-F) tumor samples in the two experimental groups (H+/T+, H−/T−) for F4/80 (A and D), arginase (B and E), and iNOS (C and F); scale bar = 50 μm. The data represent the mean (± SD) of positive cells per section (HT-1080: group H+/T+, n = 5; group H−/T−, n = 5; A549: group H+/T+, n = 5; group H−/T−, n = 4). Two-sided Student *t* test was applied for comparisons between the two groups. (**p*<0.05, ***p*<0.01). Tumors were obtained from previously published experiments (Fang et al.,

Author Manuscript Author Manuscript Author Manuscript Author Manuscript

2012). G. Analysis of gene expression array datasets of PAI-1 and CD163 genes for indicated tumors. H. Analysis of RNA-seq TCGA datasets of PAI-1 and CD163 genes in colon and bladder cancer. Two-sided t-test was used to establish the significance of the correlation coefficients.

Author Manuscript Author Manuscript Author Manuscript Author Manuscript

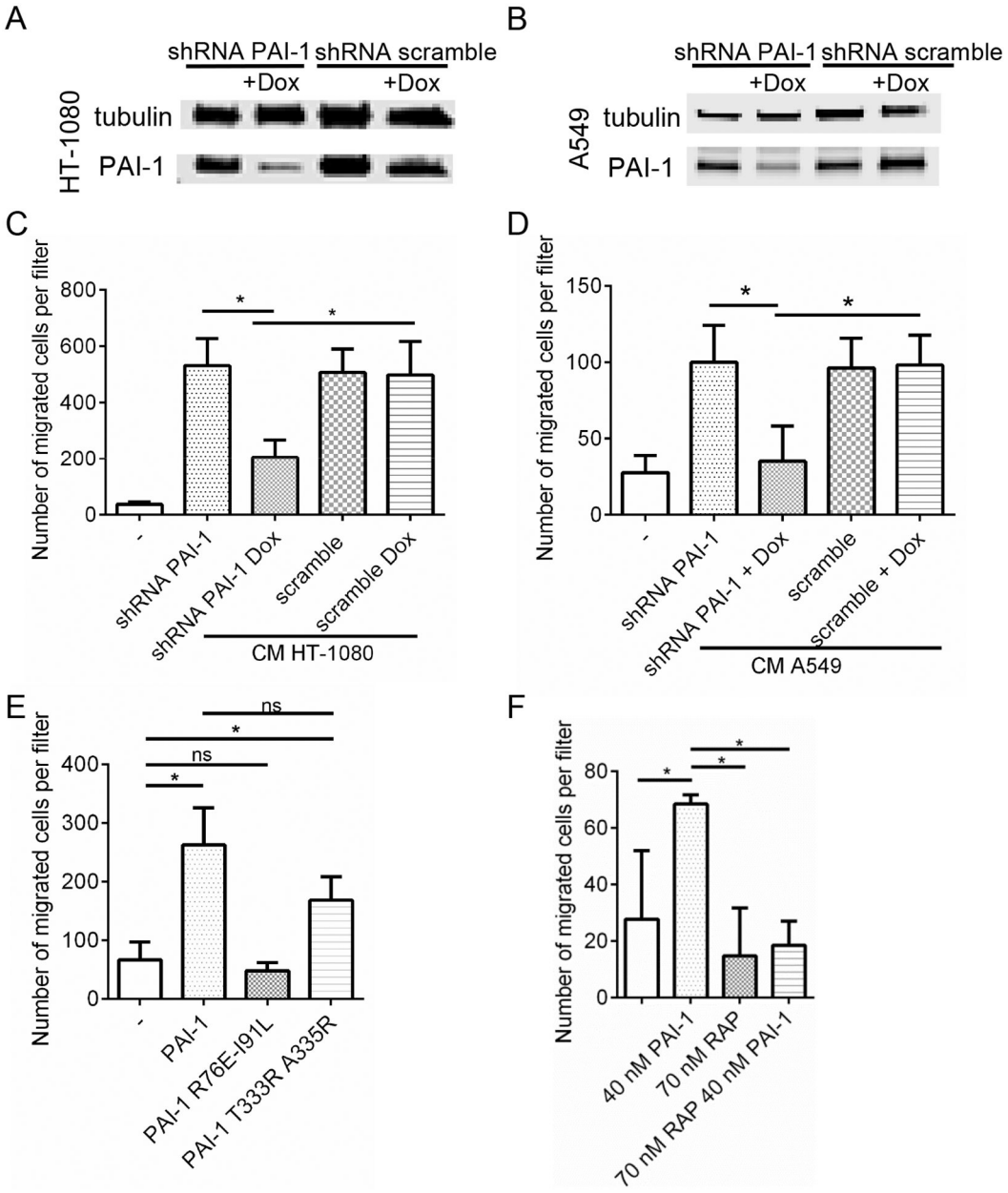

Figure 2. PAI-1 promotes macrophage migration by interacting with LRP1.

A-B. PAI-1 expression in HT-1080-Luc-shPAI1 (A), and A549-Luc-shPAI1 (B) cell lines after 3 days of doxycycline treatment. C-D. Migration of human monocytes towards conditioned medium generated from HT-1080-Luc-shPAI1 (C) and A549-Luc-shPAI1 (D) was determined using the Boyden migration assay; E-F. Migration of human monocytes in presence of rPAI-1, rPAI-1 R76E I91L, rPAI-1 T333R A335R (E) and in presence or absence of RAP (F). Data represent the mean number (± SD) of migrated cells in 9 random fields per filter in technical triplicate samples. Two-sided Student *t* test was applied for comparisons between the groups. The data from a biological duplicate experiment for E and F is presented in Figure S1.

Author Manuscript Author Manuscript Author Manuscript Author Manuscript

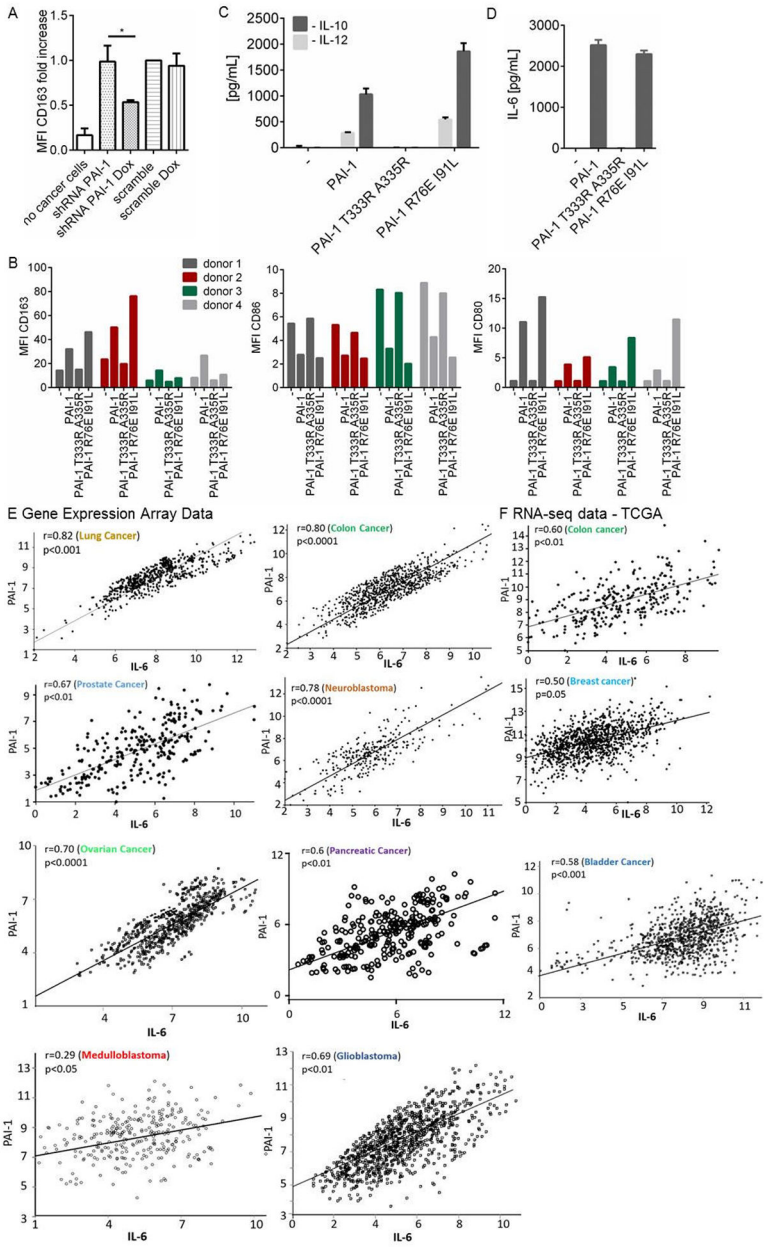

Figure 3. PAI-1 polarizes macrophages toward an M2 phenotype through its uPA interacting domain.

A. Expression of CD163 on PB monocytes was measured by FACS after 3 days in no-contact co-cultures with HT-1080-Luc-shPAI1 or HT-1080-Luc-scPAI1 cells, in the absence or presence of doxycycline. The MFIs from 2 independent experiments were normalized to the values obtained in co-cultures with HT1080-Luc-scPAI1 cells in the absence of doxycycline and averaged. Tests of difference in means between groups comprising independent, non-matched observations were based on analysis of variance (*p<0.5); B. MFIs of CD163, CD86 and CD80 on PB monocytes from 4 healthy blood donors cultured in the presence of rPAI-1, rPAI-1 R76E I91L and rPAI-1 T333R A335R (100 nM). The data represent the MFI value obtained for each independent experiment; C. Levels of IL-10 and

Author Manuscript Author Manuscript Author Manuscript Author Manuscript

IL-12 produced by PB monocytes from (B). D. Levels of IL-6 in same conditions as in (C). The data represent the mean (± SD) concentration in technical duplicate samples from four independent experiments. D-E. Analysis of GEO datasets (E) and RNA-seq TCGA datasets (F) for PAI-1 and IL-6 genes for indicated tumors. A two-way t-test was used to establish the significance of the correlation coefficients.

Author Manuscript
Author Manuscript
Author Manuscript
Author Manuscript

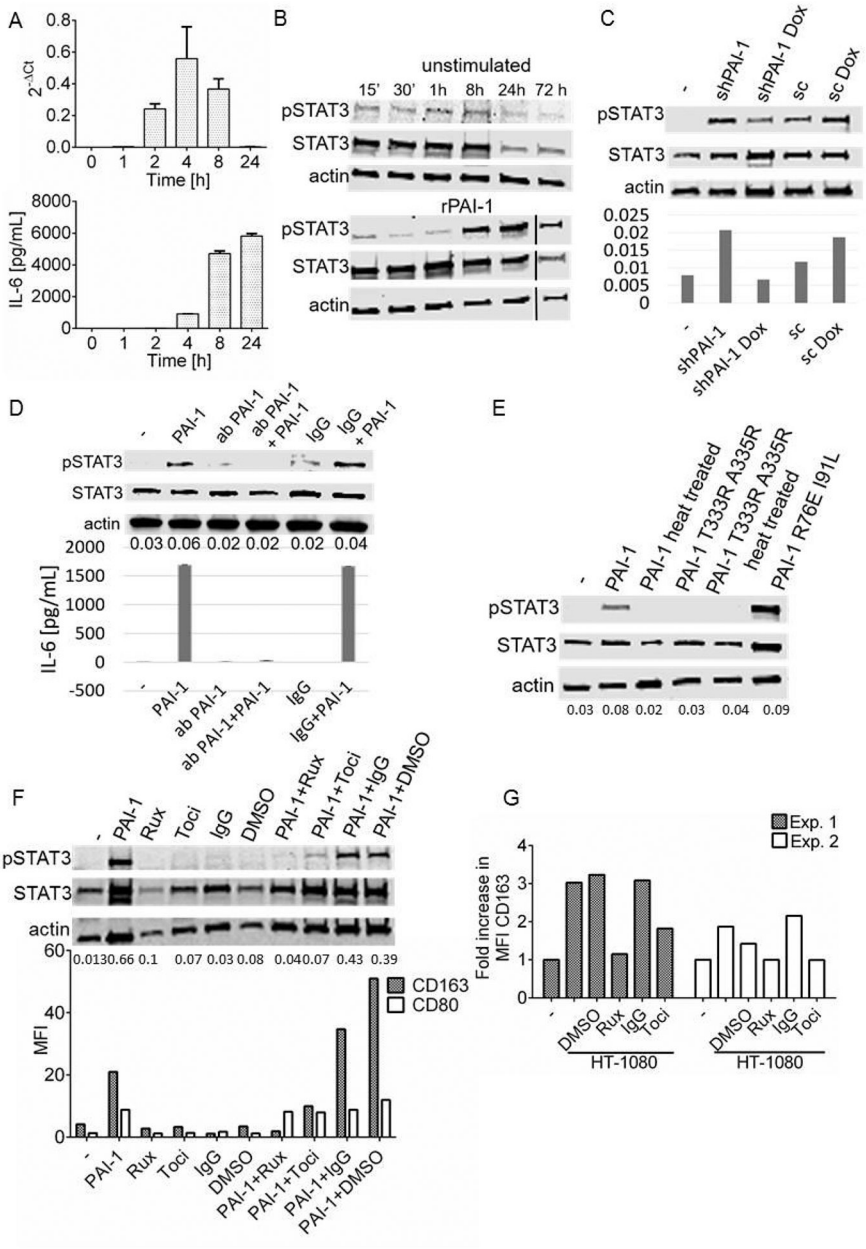

Figure 4. PAI-1-mediated macrophage polarization is IL-6- and STAT3-dependent.

A. Upper panel: IL-6 mRNA expression level measured by qRT-PCR at indicated times in PB monocytes exposed to rPAI-1 (100 nM). The data represent levels normalized against GAPDH analyzed using $2^{-\Delta Ct}$ method. Lower panel: corresponding IL-6 protein levels determined by ELISA on aliquots of the medium collected at indicated times. The data represent the mean (± SD) of technical duplicates; **B**. Western blot analysis of STAT3 phosphorylation in cell lysates of PB monocytes at indicated times after treatment with 40 nM rPAI-1; **C**. Western blot analysis of STAT3 phosphorylation (Y705) in cell lysates of PB monocytes co-cultured (no-contact) for 3 days with HT1080-Luc-shPAI1 cells in presence and absence of doxycycline. The bar diagram under each lane represents ratio of pSTAT3:STAT3; **D**. Western blot analysis of STAT3 phosphorylation of PB monocytes

Author Manuscript Author Manuscript Author Manuscript Author Manuscript

exposed to a PAI-1 blocking antibody (5 μg/mL) or isotype antibody and rPAI-1 (40 nM) for 5 h. Lower panel: IL-6 levels measured by ELISA in the medium of PB monocytes treated as indicated in the top panel. The data represent the mean IL-6 concentrations (± SD) of technical duplicates; **E**. Western blot analysis of STAT3 phosphorylation in lysates from PB monocytes cultured for 4 days in the presence of rPAI-1 and rPAI-1 mutants (40 nM). When indicated, rPAI-1 was heated for 60 min at 95°C. The numbers under each lane represent ratio of pSTAT3:STAT3; **F**. Western blot analysis of STAT3 phosphorylation in lysates of PB monocytes obtained after 6 days of treatment with rPAI-1 (40 nM), ruxolitinib (1 μM), tocilizumab (20 μg/mL), IgG (20 μg/mL) or DMSO or their combination. The numbers under each lane represent ratio of pSTAT3:STAT3. Lower panel: corresponding CD163 MFIs of PB monocytes treated as indicated in the upper panel. The data from an independent biological replicate of this experiment is shown in Figure S3; **G**. CD163 MFIs in PB monocytes after 3 days in no-contact co-cultures with HT1080 cells in the presence of DMSO, IgG, ruxolitinib or tocilizumab. The data represent the mean values of 2 independent experiments. Tests of difference in means between groups comprising independent, non-matched observations were based on analysis of variance.

Author Manuscript Author Manuscript Author Manuscript Author Manuscript

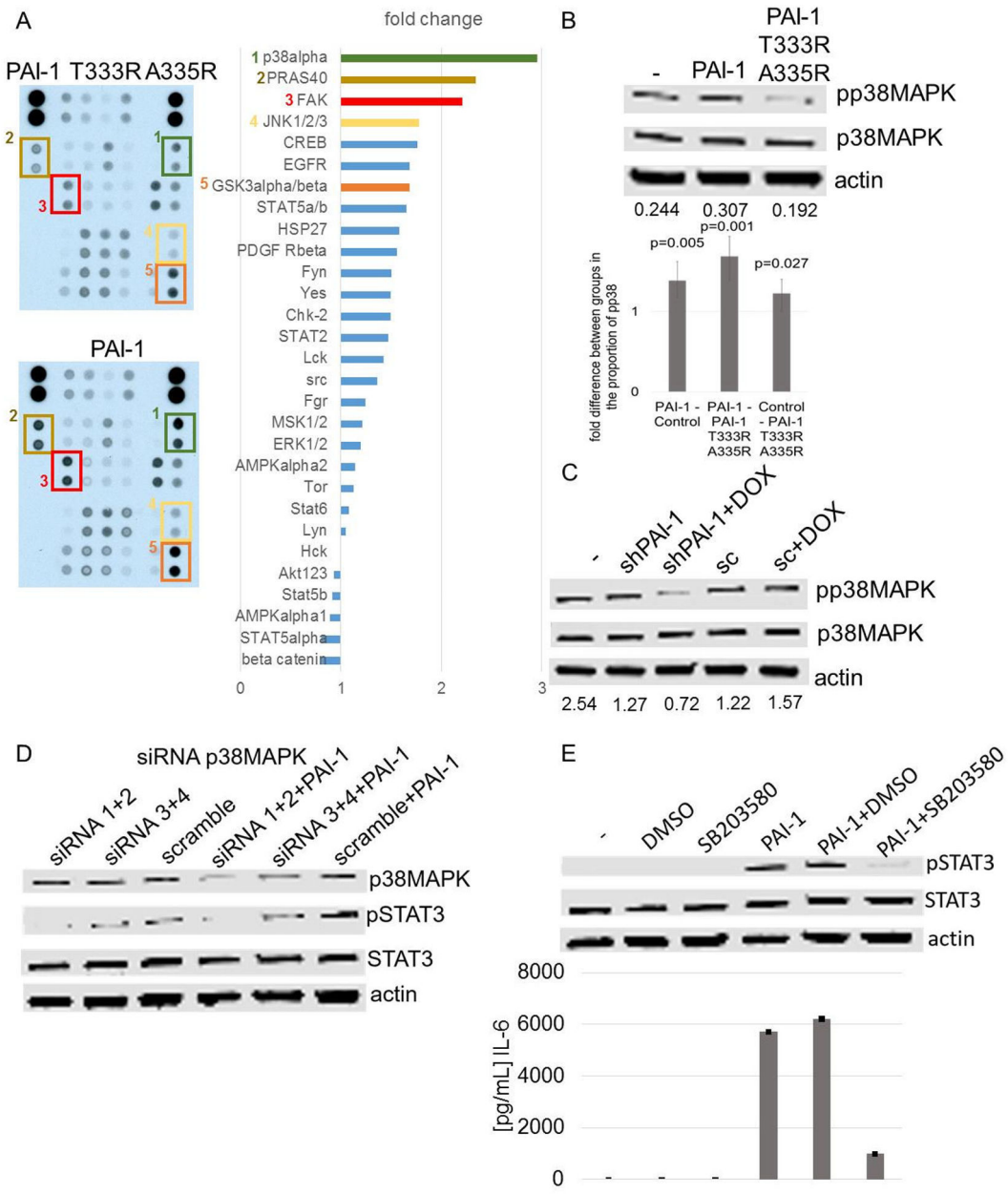

Figure 5. IL-6 and STAT3 activation by PAI-1 in monocytes is p38MAPK-dependent.

A. Phospho-Kinase Array of PB monocytes exposed to rPAI-1 and rPAI-1 T333R A335R (100 nM) for 10 min (left panel). The intensity of the signal was quantified as a fold change in signal intensity in rPAI-1-treated cells over rPAI-1 T333R A335R-treated cells (right panel); **B**. Top panel: western blot analysis of p38MAPK phosphorylation in lysates of PB monocytes obtained 10 min after exposure to rPAI-1 and rPAI-1 T333R A335R (100 nM). The data are representative of one of 3 independent experiments showing similar results. Lower panel: mean (± 95% CI) fold change in the ratio pp38MAPK:p38MAPK from 3 independent experiments. P values are based on analysis of variance of log10 ratios. **C.** Western blot analysis of phosphorylation of p38MAPK in lysates of PB monocytes 10 min after exposure to CM from HT1080-Luc-shPAI1 and HT1080-Luc-scPAI1 cultured in the

Author Manuscript Author Manuscript Author Manuscript Author Manuscript

presence or absence of doxycycline. Ratios of pp38MAPK:p38MAPK obtained by scanning densitometry are shown at the bottom of the gel. The data are representative of one of 2 independent experiments showing similar results; **D.** Western blot analysis of p38MAPK, pSTAT3 and STAT3 in PB monocytes transduced with p38MAPK siRNA and scrambled control siRNA and treated for 7 h with rPAI-1 (100 nM); **E.** Top panel: western blot analysis of pSTAT3 in PB monocytes exposed for 7 h to 100 nM rPAI-1, DMSO, or SB203580 (20 μM; 1 h preincubation) or their combination. Lower panel: IL-6 protein levels in the medium of PB monocytes under the conditions described in the top panel. The data represent the mean (± SD) of technical duplicates.

Author Manuscript Author Manuscript Author Manuscript Author Manuscript

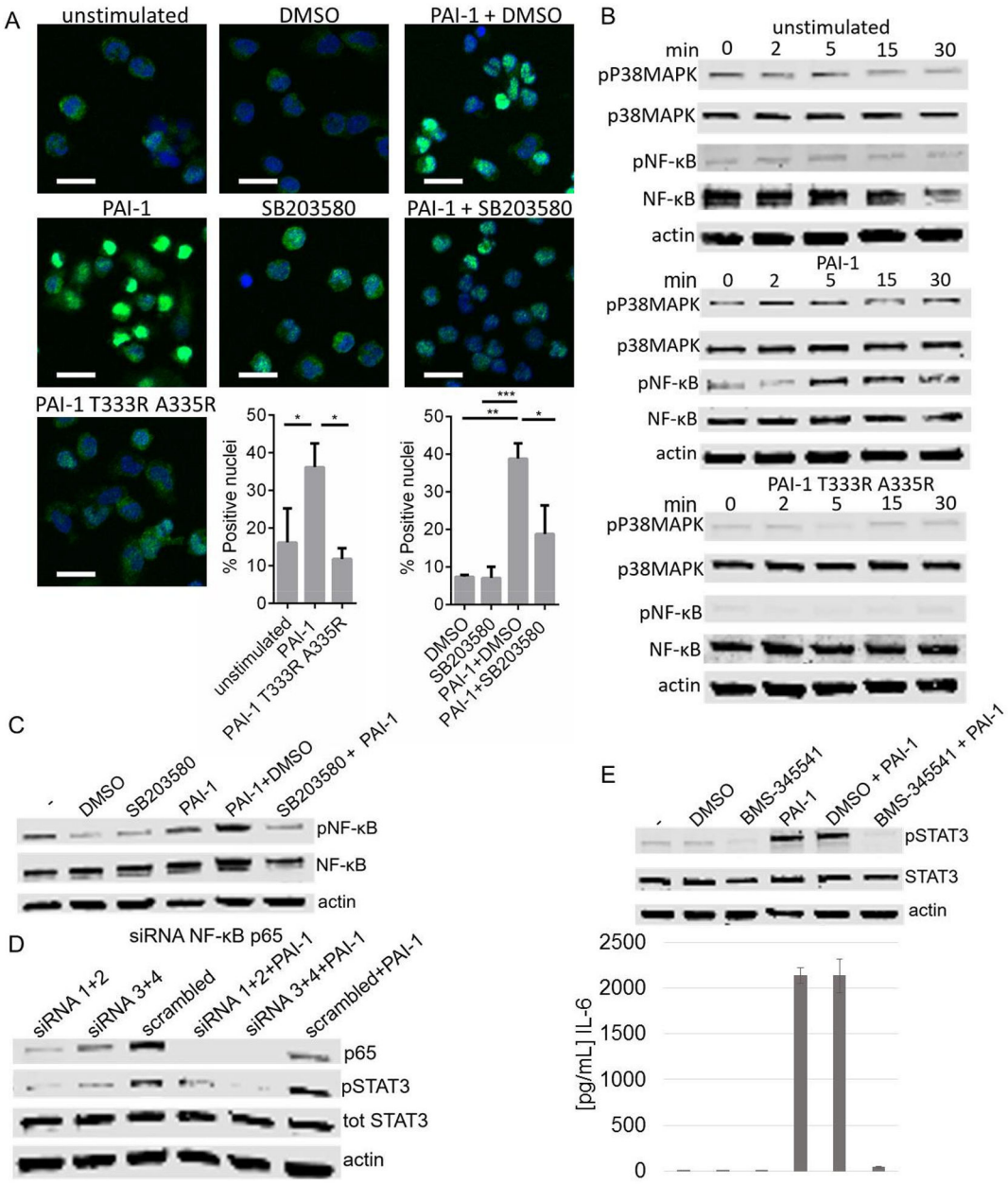

Figure 6. Induction of IL-6 by p38MAPK is NF-κB dependent.

A. Immunofluorescence (IF) analysis of PB monocytes treated with 100 nM rPAI-1 and rPAI-1 T333R A335R for 2 h. When indicated PB monocytes were preincubated with SB203580 (20 μM) for 1 h (or DMSO as a control) and treated with rPAI-1 for 2 h. Cells were analyzed by confocal microscopy for NF-κB. NF-κB: green, DAPI: blue. Scale bar: 20 μm. The histogram represents the mean (± SD) % of nuclei staining positive for NF- κB from a total of 450 nuclei per sample in triplicate (*p<0.05; **p<0.01; ***p<0.001). **B.** Western blot analysis of p38MAPK and NF-κB p65 and their phosphorylated forms in lysates of PB monocytes exposed to 100 nM rPAI-1 or rPAI-1 T333R A335R for the indicated amount of time; **C.** Western blot analysis of NF-κB p65 and its phosphorylated form in lysates of PB monocytes exposed for 7 h to rPAI-1, DMSO or SB203580 alone or

Author Manuscript Author Manuscript Author Manuscript Author Manuscript

indicated combinations; **D.** Western blot analysis of p65 NF-κB, and STAT3 and its phosphorylated form in lysates of PB monocytes in which p65 was downregulated with siRNA and exposed for 7 h to 100 nM rPAI-1; **E.** Top panel: western blot analysis of STAT3 and its phosphorylated form in lysates of PB monocytes exposed for 7 h to rPAI-1, DMSO, BMS-345541 (5 μM; 1 h pre-incubation) or their combination. Lower panel: IL-6 levels in the medium of PB monocytes treated as indicated in the top panel. The data represent the mean concentrations (± SD) of technical duplicates.

Author Manuscript Author Manuscript Author Manuscript Author Manuscript

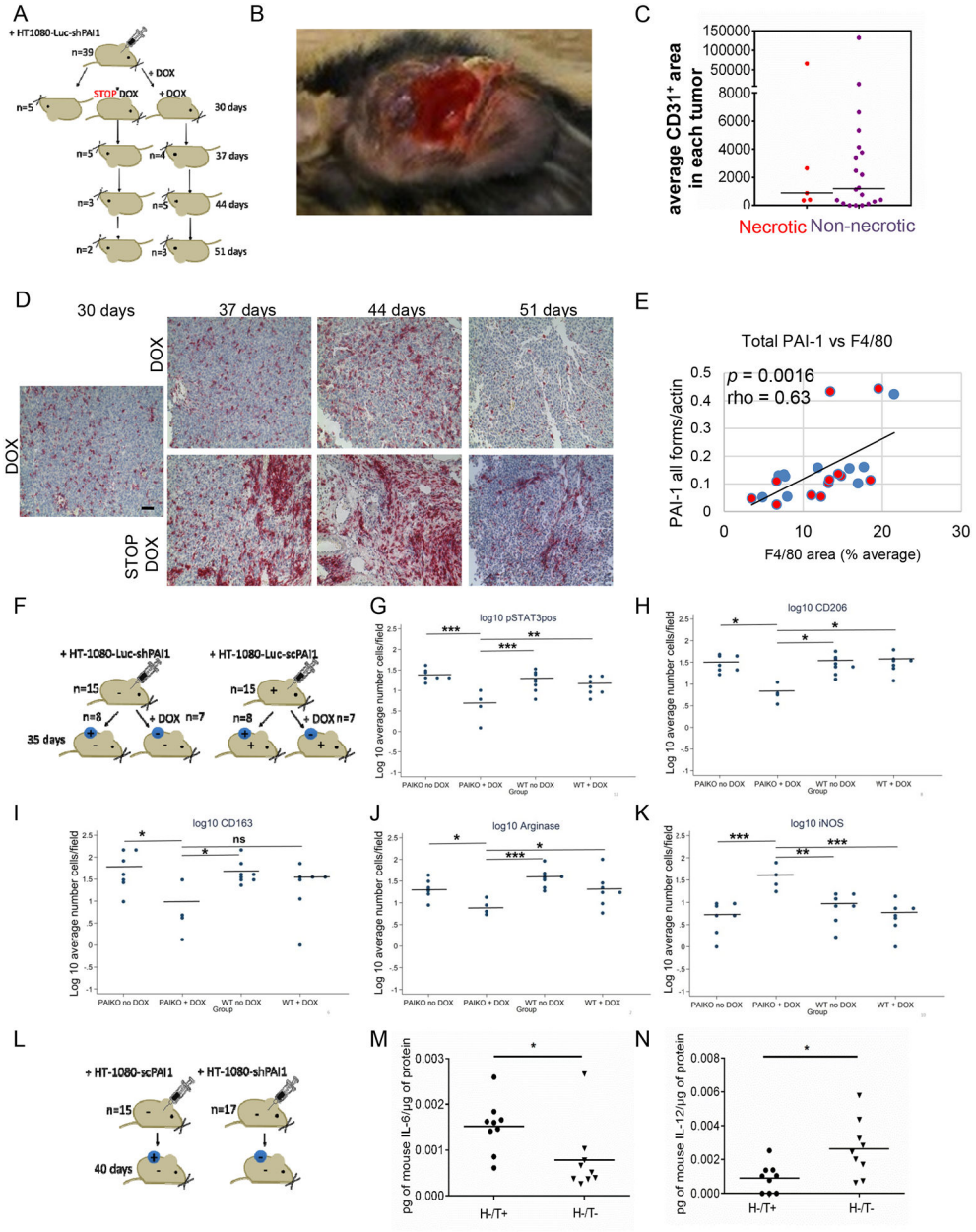

Figure 7. Tumor-derived PAI-1 increases macrophage infiltration and polarization in xenotransplanted tumors.

A. Experimental design: Rag1$^{-/-}$ PAI-1$^{-/-}$ mice (n=39) were injected with HT-1080-Luc-shPAI1. The mice received doxycycline (DOX) in drinking water for 30 days after which 5 mice were sacrificed and doxycycline was stopped in 10 of the mice (STOP DOX). In each group, mice were sacrificed at day 37 (n=9), 44 (n=8) and 51 (n=5) post-implantation, and tumors were examined for the presence of M2 macrophages (F4/80) and total PAI-1 expression. As controls, we used PAI-1$^{-/-}$ mice, injected subcutaneously with HT-1080-Luc-scrambled cells and receiving doxycycline (n=5) which were sacrificed at day 44; **B.** percent of necrotic tumors in each 3 experimental groups. Inset: photograph of a necrotic tumor **C.** Quantified average mean vascular density (CD31^{+} area) in necrotic and non-necrotic tumors;

Author Manuscript Author Manuscript Author Manuscript Author Manuscript

D. Representative IHC analysis of tumor sections at indicated times for F4/80 expression; **E.** Spearman correlation analysis of PAI-1 expression level (PAI-1/actin) vs average per cent of F4/80 positive area from IHC analysis. Each data-point represents an average of 5 sections per tumor and 5 fields per section. Red dots – mice receiving doxycycline, blue dots – mice in which doxycycline was discontinued; **F.** Experimental design: $Rag1^{-/-}$ $PAI\text{-}1^{-/-}$ mice were injected with HT-1080-Luc-shPAI1 and $Rag1^{-/-}$ $PAI\text{-}1^{+/+}$ mice were injected with HT-1080-Luc-scPAI1 tumor cells. Half of the mice received doxycycline in drinking water for 35 days (+DOX). After 35 days, mice were sacrificed and tumors were examined for the presence of macrophages and concentrations of cytokines as indicated in Methods (see also Figures S4 and S5); **G-K:** Quantitative analysis of $pSTAT3^{+}$ in $F4/80^{+}$ cells (G), $CD206^{+}$ cells (H), $CD163^{+}$ cells (I), $Arginase^{+}$ (J) and $iNOS^{+}$ (K) cells. The data represent the Log 10 average of number of positive cells. Bars indicate the mean log10 value in each group. * = $p<0.05$; ** = $p<0.1$; *** = $p<0.01$**. L:** Experimental design: $Rag1^{-/-}$ $PAI\text{-}1^{-/-}$ mice were injected with HT-1080-shPAI1 and with HT-1080-scPAI1 tumor cells. After 40 days, mice were sacrificed and tumors were examined for cytokine expression; **M-N**. Each data-point represents a technical duplicate and has been expressed as pg of cytokine per μg of protein in tumor lysate.

Author Manuscript Author Manuscript Author Manuscript Author Manuscript

KEY RESOURCES TABLE

REAGENT or RESOURCE	SOURCE	IDENTIFIER
Antibodies		
APC/Cy7 anti-human CD14 Antibody	Biolegend	Cat#325620; RRID:AB_830693
APC/Cy7 Mouse IgG1 κ Isotype Ctrl	Biolegend	Cat#400128
Alexa Fluor® 647 anti-human CD163 Antibody	Biolegend	Cat#333619; RRID:AB_2563474
Alexa Fluor® 647 Mouse IgG1, κ Isotype Ctrl	Biolegend	Cat#400130
FITC anti-human CD163 Antibody	Biolegend	Cat#333618; RRID:AB 2563094
FITC Mouse IgG1, κ Isotype Ctrl	Biolegend	Cat#400110
Brilliant Violet 605™ anti-human CD86 Antibody	Biolegend	Cat#305429; RRID:AB_11203889
Brilliant Violet 605™ Mouse IgG2b, κ Isotype Ctrl	Biolegend	Cat#400349
PE anti-human CD80 Antibody	Biolegend	Cat#305208; RRID:AB_314504
PE Mouse IgG1, κ Isotype Ctrl	Biolegend	Cat#400112
Human TruStain FcX	Biolegend	Cat#422302
Anti-Actin antibody produced in rabbit	Sigma Aldrich	Cat#A2066; RRID:AB_476693
Monoclonal Anti-β-Tubulin antibody produced in mouse	Sigma-Aldrich	Cat#T4026; RRID:AB_477577
Human Serpin E1/PAI-1 Antibody goat anti-human	R&D Systems	Cat#AF1786; RRID:AB_2187024
Human gp130 PE-conjugated Antibody	R&D Systems	Cat#FAB228P-025
Human IL-6 R alpha Fluorescein-conjugated Antibody	R&D Systems	Cat#FAB227F-025
Phospho-Stat3 (Tyr705) Antibody	Cell Signaling	Cat#9131; RRID:AB_331586
Stat3 (79D7) Rabbit mAb	Cell Signaling	Cat#4904
Phospho-p38 MAPK (Thr180/Tyr182) (D3F9) XP® Rabbit mAb	Cell Signaling	Cat#4511; RRID:AB_2139682
p38 MAPK Antibody	Cell Signaling	Cat#9212; RRID:AB_330713
Phospho-NF-KB p65 (Ser536) (93H1) Rabbit mAb	Cell Signaling	Cat#3033; RRID:AB_331284
NF-κB p65 (D14E12)XP (R) Rabbit mAb	Cell Signaling	Cat#8242; RRID:AB_10859369
Unconjugated rabbit anti-rat IgG Antibody	Vector Laboratories	Cat#AI-4000
Goat Biotinylated anti-rabbit IgG (H+L)	Vector Laboratories	Cat#BA-1000; RRID:AB_2313606
Goat Biotinylated anti-rat IgG (H+L)	Vector Laboratories	Cat#BA-9400; RRID:AB_2336202
DyLight 488 anti-rabbit IgG	Vector Laboratories	Cat#DI-1488; RRID:AB_2336402
Anti-F4/80 Antibody	Abcam	Cat#ab6640; RRID:AB_1140040

Author Manuscript Author Manuscript Author Manuscript Author Manuscript

REAGENT or RESOURCE	SOURCE	IDENTIFIER
Anti-iNOS antibody	Abcam	Cat#ab15323; RRID:AB_301857
Anti-pSTAT3 antibody	Cell Signaling	Cat#9145L
Anti-CD206 antibody	Abcam	Cat#64693
goat anti-rabbit 800CW	LI-COR	Cat#926–32211; RRID:AB_621843
donkey anti-mouse 680LT	LI-COR	Cat#926–68022; RRID:AB_10715072
donkey anti-goat 800CW	LI-COR	Cat#926–32214; RRID:AB_621846
donkey anti-goat 680LT	LI-COR	Cat#926–68024; RRID:AB_10706168
Anti-arginase I Antibody (H-52)	Santa Cruz	Cat#sc20150; RRID:AB_2058955
Cy™3 AffiniPure Donkey Anti-Rat IgG (H+L)	Jackson ImmunoResearch	Cat#712-165-153; RRID:AB_2340667
Anti-human PAI (inhibitory) antibody	Molecular Innovations	Cat#MA-8H9D4
LEAFtm Purified Mouse IgG1 K isotype cntr	Biolegend	Cat#400124
Bacterial and Virus Strains		
Biological Samples		
Chemicals, Peptides, and Recombinant Proteins		
puromycin	Sigma-Aldrich	Cat#P9620
Histopaque	Sigma-Aldrich	Cat#10771–500ML
0.1% Poly-L-Lysine solution	Sigma-Aldrich	Cat#P8920
Sodium butyrate	Sigma-Aldrich	Cat#B5887
BMS-345541	Sigma-Aldrich	Cat#B9935–5MG
Doxycycline hyclate	Sigma-Aldrich	Cat#D9891–25g
4-(2-hydroxyethyl)-1-piperazineethanesulfonic acid (HEPES)	Sigma-Aldrich	Cat#H3375
Penicillin-Streptomycin (10,000 U/mL)	Gibco	Cat#15140–122
Cell Dissociation buffer, Enzyme free, PBS	Gibco	Cat#13151–014
Geneticin	Gibco	Cat#10131-035
Falcon® Permeable Support for 24 Well Plate with 8.0μm Transparent PET Membrane	Corning	Cat#353097
Dulbecco's Modified Eagle's Medium (DMEM)	Corning	Cat#10-013-CV
phosphate-buffered saline (PBS)	Corning	Cat#21–031-CV
Roswell Park Memorial Institute (RPMI)	Corning	Cat#10-040-CV

Author Manuscript Author Manuscript Author Manuscript Author Manuscript

REAGENT or RESOURCE	SOURCE	IDENTIFIER
DAPI	Thermo Fisher Scientific	Cat#D21490
HaltTM Protease and Phosphatase inhibitor single use cocktail	Thermo Fisher Scientific	Cat#78442
AmpFLSTR Identifiler PCR Kit	Thermo Fisher Scientific	Cat#4322288
Human PAI-1 (stable mutant form)	Molecular Innovations	Cat#CPAI
Human PAI-1 (stable mutant, no LRP binding)	Molecular Innovations	Cat#HPAI-R76E-I91L
Human PAI-1 (substrate form - P12 Arginine P14 Arginine double mutant)	Molecular Innovations	Cat#HPAI-RR
Low Endotoxin Human RAP	Molecular Innovations	Cat#RAP-LE
Vectashield antifade mounting medium with DAPI	Vector Laboratories	Cat#H-1200
Vectastain ELITE ABC-HRP peroxidase kit	Vector Laboratories	Cat#PK-6100
Antigen unmasking solution	Vector Laboratories	Cat#H-3300
Bloxall	Vector Laboratories	Cat#SP-6000
ImmPACTTM DAB	Vector Laboratories	Cat#SK-4105
Methyl Greene	Vector Laboratories	Cat#H-3402
Tris(hydroxymethyl)aminomethane (Tris)	Invitrogen	Cat#15504-020
Lipofectamine 2000	Invitrogen	Cat#11668019
ER retrieval solution pH 6.0 BOND Novocastra	Leica	Cat#RE7113-CE
Bond Polymer Refine Red detection kit	Leica Biosystems	Cat#DS9390
Actemra (Tocilizumab)	Genentech	Cat#NDC 50242135-01
Tiplaxtinin	Axon Medchem	Cat#Axon1383
4–15% Mini-Protean® TGXTM Precast Protein gels	BIO-RAD	Cat#456-1084
siLentFectTMLipid Reagent for RNAi,0.5 ml	BIO-RAD	Cat#1703360
Ruxolitinib	Selleckchem	Cat#S1378
0.45 μM syringe filters	VWR International	Cat#28145-479
SB203580	Cell Signaling	Cat#5633
Cytoseal XYL	Richard-Allan Scientific	Cat#8312-4
EasySepTM Human Monocyte Enrichment Kit	StemCell	Cat#19059
Odyssey Blocking Buffer (PBS)	LI-COR	Cat#927-40000
Proteinase K, recombinant PCR grade	Roche	Cat#03115828001
Fetal Bovine Serum (Tetracycline-free)	Omega Scientific	Cat#FB-15
Hema 3 stain set for Wright-Giemsa stain	Protocol	Cat#123–869
MycoAlert Mycoplasma detection kit	Lonza	LT07-118
Critical Commercial Assays		
Human IL-12/IL-23 p40 DuoSet, 5 Plate	R&D Systems	Cat#DY1240-05
Human IL-10 DuoSet,5 Plate	R&D Systems	Cat#DY217B-05
Human IL-6 DuoSet, 15 Plate	R&D Systems	Cat#DY206
Mouse IL-10 DuoSet ELISA	R&D Systems	Cat#DY417-05
Proteome Profiler Human Phospho-Kinase Array Kit	R&D Systems	Cat#ARY003B

Author Manuscript Author Manuscript Author Manuscript Author Manuscript

REAGENT or RESOURCE	SOURCE	IDENTIFIER
EndoLISA® ELISA-based Endotoxin Detection Assay	Hyglos	Cat#609033
SuperScript® III First-Strand Synthesis System	Invitrogen	Cat#18080-051
Taqman IL-6 assay 4331182	Applied Biosystems	Cat#Hs00985639_m1
Taqman GAPDH assay 4331182	Applied Biosystems	Cat#Hs03929097_g1
TaqMan® Universal Master Mix II, no UNG	Applied Biosystems	Cat#4440040
Taqman ACTB assay 4331182	Applied Biosystems	Cat#Hs99999903_m1
Taqman 18S assay 4453320	Applied Biosystems	Cat#Hs99999901_s1
Deposited Data		
Experimental Models: Cell Lines		
Human Embryonic Kidney 293 cells	ATCC	Cat#CRL-1573
HT-1080 [HT1080] ATCC CCL-121TM	ATCC	Cat#CCL-121
A549	Lieber et al., 1976	N/A
Experimental Models: Organisms/Strains		
Rag1−/− PAI-1−/− and Rag1−/− PAI-1+/+ immunodeficient female and male mice were obtained by mating PAI-1- deficient mice (PAI-1−/−) and their corresponding wild- type mice (PAI-1+/+) on a mixed genetic background of 87% C57BL/6 and 13% 129 strain [25] with Rag-1- deficient mice (Rag-1−/−: B6; 129 s-Rag-1tm/Mom/J) [26].	Carmeliet et al., 1993 Bajou et al., 2008	N/A
Oligonucleotides		
ON-TARGET plus Set of 4 siRNA MAPK14	Dharmacon	J-003512-20
ON-TARGET plus Set of 4 siRNA MAPK14	Dharmacon	J-003512-20
ON-TARGET plus Set of 4 siRNA MAPK14	Dharmacon	J-003512-20
ON-TARGET plus Set of 4 siRNA MAPK14	Dharmacon	J-003512-20
ON-TARGET plus Set of 4 siRNA NF-κB p65	Dharmacon	J-003533-06
ON-TARGET plus Set of 4 siRNA NF-κB p65	Dharmacon	J-003533-06
ON-TARGET plus Set of 4 siRNA NF-κB p65	Dharmacon	J-003533-06
ON-TARGET plus Set of 4 siRNA NF-κB p65	Dharmacon	J-003533-06
ON-TARGET plus Non-targeting control	Dharmacon	D-001810-10-05
shPAI-1 5′-CCGGCAGACAGTTTCAGGCTGACTTCTCGAGAAGTCAGCCTGAAACTGTCTGTTTTT-3′		TRCN0000052271

Author Manuscript Author Manuscript Author Manuscript Author Manuscript

REAGENT or RESOURCE	SOURCE	IDENTIFIER
shPAI-2 5′-AATTAAAAACAGACAGTTTCAGGCTGACTTCTCGAGAAGTCAGCCTGAAACTGTCTG-3′		TRCN0000052271
Scramble 1 5′-CCGGAATTCTCCGAACGTGTCACGTCTCGAGACGT		N/A
GACACGTTCGGAGAATTTTTTT-3′		
Scramble 2 5′-AATTAAAAAAATTCTCCGAACGTGTCACGTCTCGAGACGTGACACGTTCGGAGAATT-3′		N/A
Recombinant DNA		
Tet-pLKO-puro lentiviral vector	Wee et al., 2008; Wiederschain et al., 2009	Addgene Cat#21915
psPAX2	Gift from Didier Trono lab	Addgene Cat#12260
pMD2.G	Gift from Didier Trono lab	Addgene Cat#12259
Software and Algorithms		
Other		